ARTICLE

MicroRNA-directed pathway discovery elucidates an miR-221/222–mediated regulatory circuit in class switch recombination

Eric J. Wigton[1,2] , Yohei Mikami[3,4] , Ryan J. McMonigle[5] , Carlos A. Castellanos[1,2] , Adam K. Wade-Vallance[1,10,11] , Simon K. Zhou[1,2] , Robin Kageyama[1,2,6] , Adam Litterman[1,2] , Suparna Roy[1,7] , Daisuke Kitamura[8] , Emily C. Dykhuizen[9] , Christopher D.C. Allen[1,10,11] , Hui Hu[5] , John J. O'Shea[3] , and K. Mark Ansel[1,2]

MicroRNAs (miRNAs, miRs) regulate cell fate decisions by post-transcriptionally tuning networks of mRNA targets. We used miRNA-directed pathway discovery to reveal a regulatory circuit that influences Ig class switch recombination (CSR). We developed a system to deplete mature, activated B cells of miRNAs, and performed a rescue screen that identified the miR-221/222 family as a positive regulator of CSR. Endogenous miR-221/222 regulated B cell CSR to IgE and IgG1 in vitro, and miR-221/222–deficient mice exhibited defective IgE production in allergic airway challenge and polyclonal B cell activation models in vivo. We combined comparative Ago2-HITS-CLIP and gene expression analyses to identify mRNAs bound and regulated by miR-221/222 in primary B cells. Interrogation of these putative direct targets uncovered functionally relevant downstream genes. Genetic depletion or pharmacological inhibition of *Foxp1* and *Arid1a* confirmed their roles as key modulators of CSR to IgE and IgG1.

Introduction

MicroRNAs (miRNAs, miRs) are 18–22-nt small noncoding RNAs that post-transcriptionally inhibit the expression of their target genes (Bartel, 2004). miRNAs target mRNAs via complementary base pairing to the 3′ untranslated region (UTR). Families of miRNAs with shared target repertoires are defined by their "seed sequence" (nt 2–8 from the 5′ end of the mature miRNA), which is the major determinant of target recognition (Jonas and Izaurralde, 2015). They guide the Argonaute (Ago) protein-containing miRNA-induced silencing complex (miRISC) to mRNA targets based on this seed sequence identity (Bartel, 2004). The miRISC mediates translational inhibition and destabilization of bound mRNAs (Jonas and Izaurralde, 2015). Individual miRNAs and their family members can target hundreds of unique transcripts and thereby regulate large gene networks in a manner specific to cellular context and gene expression program. This form of post-transcriptional gene network regulation has proved to be indispensable for cellular

development and function in a wide diversity of multicellular animals.

In the context of the immune system, miRNAs are necessary for B cell development from the pro–B cell to pre–B cell stage because B cell lineage–specific ablation of the miRNA processing enzyme Dicer leads to a complete block at this developmental stage (Koralov et al., 2008). Further studies identified individual miRNAs and miRNA families that are necessary for key developmental checkpoints in B cell lineage commitment (Coffre and Koralov, 2017). Dicer ablation later in B cell maturation leads to a lupus-like disease and a skewing of the Ig repertoire toward reactivity against a multitude of self-antigens (Belver et al., 2010). Several individual miRNA families have been shown to regulate B cell activation and function in immune responses, including their participation in germinal centers and the generation of antibody-producing plasma cells (de Yébenes et al., 2008; Rodriguez et al., 2007; Thai et al., 2007; Vigorito et al.,

[1]Sandler Asthma Basic Research Center, University of California, San Francisco, San Francisco, CA; [2]Department of Microbiology & Immunology, University of California, San Francisco, San Francisco, CA; [3]Molecular Immunology and Inflammation Branch, National Institute of Arthritis and Musculoskeletal and Skin Diseases, National Institutes of Health, Rockville, MD; [4]Division of Gastroenterology and Hepatology, Department of Internal Medicine, Keio University School of Medicine, Tokyo, Japan; [5]Department of Microbiology, University of Alabama at Birmingham, Birmingham, AL; [6]Parker Institute for Cancer Immunotherapy, San Francisco, CA; [7]Department of Dermatology, University of California, San Francisco, San Francisco, CA; [8]Research Institute for Biomedical Sciences, Tokyo University of Science, Chiba, Japan; [9]Department of Medicinal Chemistry and Molecular Pharmacology, Purdue University, West Lafayette, IN; [10]Cardiovascular Research Institute, University of California, San Francisco, San Francisco, CA; [11]Department of Anatomy, University of California, San Francisco, San Francisco, CA.

Correspondence to K. Mark Ansel: mark.ansel@ucsf.edu.

2007; Xu et al., 2015). In addition, miRNA dysregulation has been implicated in B cell malignancies, with some miRNAs acting as tumor suppressors (e.g., miR-15/16 in chronic lymphocytic leukemia) and others as oncogenes (e.g., miR-19 in lymphomagenesis). Together, these findings distinguish miRNAs as key regulators of B cell development and immune function, and their dysregulation as causation for B cell malignancy, autoimmunity, and hypersensitivity. Illuminating the gene networks that miRNAs control in B cells may provide insights into the molecular mechanisms that underlie these diseases.

miRNAs have been leveraged as discovery tools to elucidate genes and pathways that regulate lymphocyte fate and function in immunity. Rescue screens in miRNA-deficient T cells uncovered specific miRNAs that influence cytokine production (Pua et al., 2016; Steiner et al., 2011). Algorithms that use seed sequence matching and other 3′ UTR sequence features are used to predict target gene networks (Agarwal et al., 2015), and these networks can be further filtered for miRNA effects on gene expression in the appropriate cellular context (Pua et al., 2016). Ago2 high-throughput sequencing of RNA isolated by crosslinking immunoprecipitation (Ago2-HITS-CLIP) provides context-specific biochemical evidence for miRISC occupancy of potential target sites, and comparing Ago2-HITS-CLIP in miRNA-deficient and -sufficient cells facilitates mapping of specific miRNA–target interactions (Chi et al., 2009; Gagnon et al., 2019; Loeb et al., 2012). Functional interrogation of these targets can unearth regulatory genes and pathways previously unknown to be important to biological processes of interest and direct researchers to novel therapeutic targets.

Elevated production of antibodies of the IgE isotype is a hallmark of allergy (Hu et al., 2018). IgE is directly involved in the pathogenesis of asthma and other allergic diseases because it arms mast cells and basophils for rapid allergen-specific inflammatory responses (Galli and Tsai, 2012). Omalizumab, an approved therapeutic antibody that targets IgE, reduces asthma exacerbations in a subset of patients (Busse et al., 2001). It has been suggested that therapies that target or reduce the generation of IgE-producing B cells may provide better protection against symptoms of allergic diseases (Hu et al., 2018). The generation of IgE-producing B cells from naive B cells requires the induction of Ig class switch recombination (CSR), a process of somatic DNA mutation and recombination that preserves the B cell's antibody specificity while switching the isotype of its heavy chain (Yewdell and Chaudhuri, 2017; Yu and Lieber, 2019).

CSR requires multiple coordinated processes starting with active transcription driven by cytokine signaling (Stavnezer and Schrader, 2014), expression and regulation of the activation-induced cytidine deaminase (AID) enzyme, DNA repair (Yu and Lieber, 2019), and distinct regulation of the cell cycle and proliferation (Hodgkin et al., 1996). AID is directly regulated by miRNAs, specifically miR-155 (Dorsett et al., 2008; Teng et al., 2008; Vigorito et al., 2007). CSR to the IgE isotype requires IL-4 signaling, whereas CSR to IgG1 is positively influenced by, but does not necessarily require, IL-4 signaling (Finkelman et al., 1990; Kopf et al., 1993; Kühn et al., 1991). Signaling from T

follicular helper cells through CD40, and other cytokines also regulate this process (Kawabe et al., 1994; Nonoyama et al., 1993; Yang et al., 2020).

In this study, we developed a mouse model system to ablate miRNA processing in mature B cells and then performed a rescue screen for miRNAs that regulate CSR. This screen identified miR-221/222, an miRNA family previously unstudied in mature, nonmalignant B cells, as a positive regulator of this process (Knoll et al., 2013; Lupini et al., 2013; Petkau et al., 2018). We characterized miR-221/222–deficient B cells from gene-targeted mice in vitro and in vivo and empirically defined direct targets of these miRNAs in B cells through a combination of bioinformatic, biochemical, and gene expression analyses. miR-221/222 promoted CSR and B cell proliferation in vitro, IgE production in an allergic airway hypersensitivity model, and IgE[+] plasma cell generation in a model of global B cell activation. Among the targets of miR-221/222, we uncovered *Foxp1* and *Arid1a* as regulators of CSR. Together, these findings establish miR-221/222 as a regulator of B cell production of antibodies associated with allergy and asthma and provide insight into new regulators of CSR.

Results

Development of a system to interrogate miRNA regulation of CSR

In prior work, we devised an arrayed screening approach to identify miRNAs that regulate helper T cell differentiation and effector function (Pua et al., 2016; Steiner et al., 2011). This approach allowed us to isolate the function of individual miRNAs by transfecting each one into T cells that lack endogenous miRNAs due to induced genetic deficiency for the miRNA biogenesis factor Dgcr8. For this study, we extended this approach to interrogate miRNA function in B cells. *Dgcr8* can be deleted with high penetrance during late stages of T cell development, but B cells exhibit a developmental defect at the pro–B cell to pre–B cell transition in the absence of miRNA biogenesis machinery (Koralov et al., 2008). To study the role of miRNAs in regulating CSR, we bred Cγ1-Cre Dgcr8^{fl/fl} Rosa26-LSL-YFP mice to allow inducible *Dgcr8* inactivation in B cells upon activation of the Ighg1 germline transcript promoter. Splenic B cells from these mice were stimulated with mitogenic anti-CD180 crosslinking antibody and low-dose IL-4 (1 ng/ml) for 48 h (days −2–0) to force expression of Cre recombinase and inactivate *Dgcr8* without inducing CSR, then they were transferred to classical CSR conditions of LPS and high-dose IL-4 (25 ng/ml) for an additional 48–96 h (days 0–4; Fig. 1 A). Thereafter, we analyzed viability, YFP as a reporter of Cre activity, and surface IgD and IgG1 expression by flow cytometry. In these cultures, 95% of viable cells expressed YFP at day 2, indicating Cre recombinase activity in a majority of activated cells (Fig. 1 B, left panel). Importantly, these cells remained capable of undergoing CSR (Fig. 1 B, right panel).

To validate *Dgcr8* ablation, we isolated RNA from Cγ1-Cre Rosa26-LSL-YFP B cells that were also Dgcr8^{fl/fl} (D8-KO), Dgcr8^{fl/+} (D8-HET), or Dgcr8^{+/+} (D8-WT) to measure *Dgcr8* transcripts and mature miRNAs throughout the stimulation timeline. *Dgcr8* mRNA
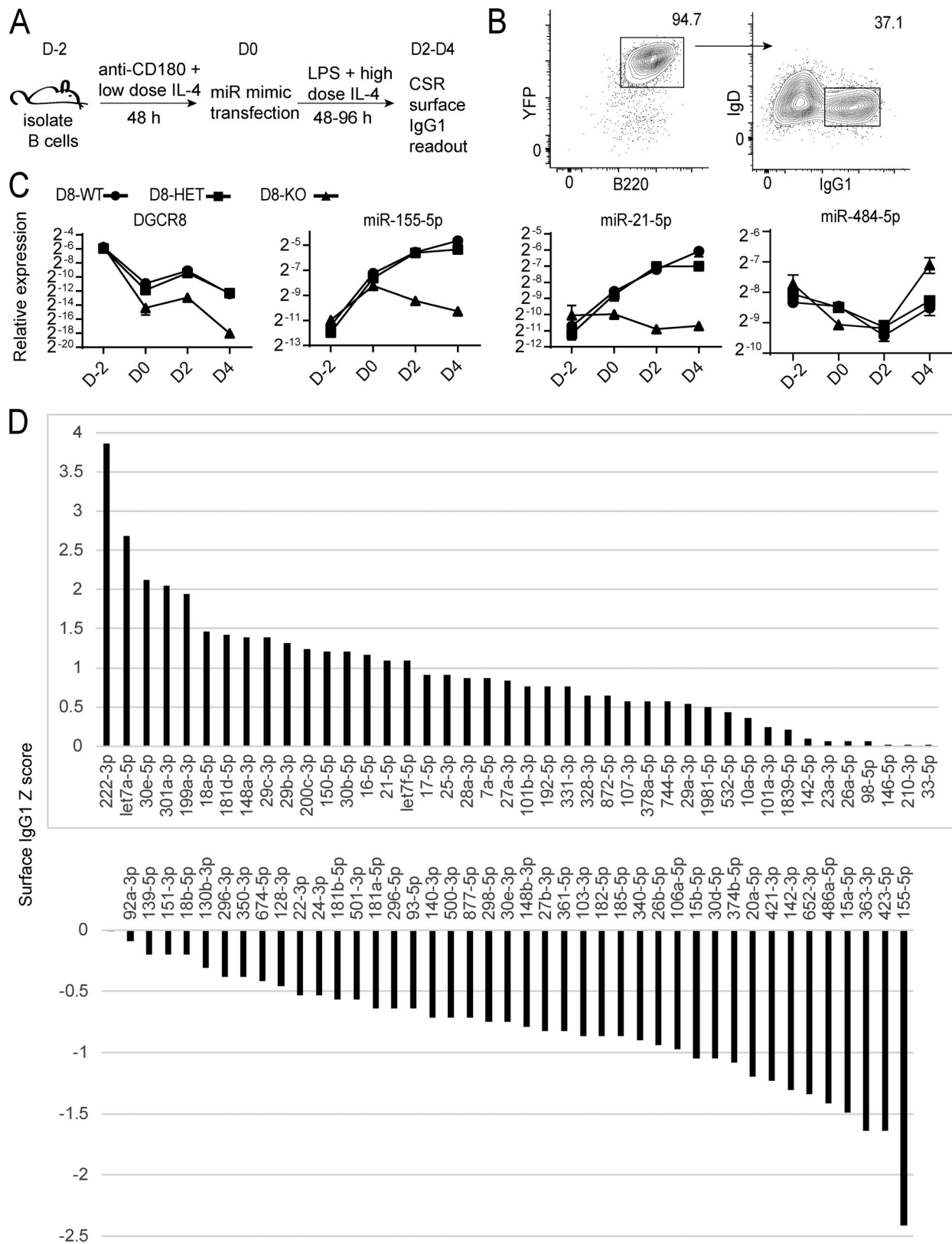
Figure 1. **Development of miRNA rescue screen in mature B cells stimulated to CSR to IgG1 implicates miR-222 as a regulator. (A)** Timing and stimulation conditions to induce Cγ1-Cre deletion of *Dgcr8* and transfect miRNA and analyze CSR by flow cytometry. **(B)** Representative flow plot of gating strategy for YFP reporter and IgG1 surface expression at day 2 during activation. **(C)** RT-qPCR of D8-WT, D8-HET, D8-KO B cell *Dgcr8* mRNA and miRNA expression throughout culturing (*Dgcr8* normalized to *Gapdh*, miRNAs normalized to small nuclear RNA U6). Data are the average of two mice from each genotype. **(D)** Screen results from the individual miRNA rescue transfections performed at day 0 and read out by flow cytometry at the day 2 time point. Z-score was calculated by $z = (x_1 - x_n)/\sigma$, where x_1 is the specific IgG1 percentage, x_n is the mean of all surface IgG1 percentages, and σ is the SD. Control bar is the average of six transfections ranging from +1 to −1 Z-score averaged.

abundance was decreased by eightfold in the D8-KO cells compared with D8-HET and D8-WT cells after the initial 2-d stimulation and continued to decrease through day 4, whereas DGCR8 appeared to be regulated by activation conditions as well (Fig. 1 C). Furthermore, the activation-induced miRNAs mmu-miR-155-5p and mmu-miR-21-5p had a 2- to 16-fold decreased expression in D8-KO compared with D8-HET and D8-WT cells, consistent with loss of Dgcr8-dependent miRNA processing activity (Fig. 1 C). In contrast, mmu-miR-484-5p was unaffected throughout the stimulation and increased at day 4 (Fig. 1 C), consistent with previous reports that Dgcr8-independent miRNAs increase in abundance in the absence of Dgcr8-dependent miRNA biogenesis (Babiarz et al., 2008).

Using these stimulation conditions, we tested the role of 85 miRNAs that are expressed in naive, activated, and/or germinal center B cells to determine miRNAs that modulate CSR in vitro (Fig. 1 D; Fowler et al., 2015; Kuchen et al., 2010; Zhang et al., 2009). We transfected B cells using the Neon next-generation transfection system (Pua et al., 2016; Steiner et al., 2011) to introduce individual miRNA mimics into D8-KO activated B cells at day 0 and measured CSR to IgG1 at day 2. These optimized conditions achieved close to 100% transfection efficiency with small RNAs, as indicated by uniform down-regulation of CD45 in cells transfected with an siRNA against its transcript, Ptprc (Fig. S1 A). Surface IgG1 expression implicated miR-155-5p as a negative regulator of CSR to IgG1 (Fig. 1 D), consistent with previous studies demonstrating that mutation of the miR-155 binding site in the Aicda 3′ UTR led to an increase in transcript, protein, and double-stranded break induction in activated B cells (Dorsett et al., 2008; Teng et al., 2008). Similarly, congruent with a previous study, miR-18a positively regulated CSR (Xu et al., 2015). Interestingly, miR-222-3p was the most potent positive modulator of IgG1 surface expression (Fig. 1 D). This miRNA and its family member miR-221-3p have been implicated in early B cell development and homing to the bone marrow (Knoll et al., 2013; Petkau et al., 2018), but not in CSR or B cell activation. In a rescreen of the top 10 and bottom 10 regulating miRNAs and their family members, both miR-222-3p and miR-221-3p increased CSR compared with control mimic (CM; Fig. S1 C). Given this consistent and robust effect, we decided to further investigate the role of the miR-221/222 family in CSR and processes that influence CSR.

Germline deletion of the miR-221/222 cluster on the X chromosome does not alter B cell development

In both mice and humans, miR-221 and miR-222 are processed from a single primary miRNA transcribed from the Mirc53 locus on chromosome X. We generated mmu-miR-221/222–deficient mice. We inserted loxP sites flanking miR-221 and miR-222 by gene targeting to create a conditional mutant allele (flox) that can be irreversibly converted to a deleted allele (Δ) upon introduction of Cre recombinase. B cells from WT and flox mice expressed equivalent amounts of miR-221-3p and miR-222-3p, and these miRNAs were undetectable in B cells from Δ mice generated by Cre expression in the germline, as determined by differential Ago2-HITS-CLIP (see Fig. 5 C). In all further experiments, we compared mice with these two targeted alleles to

determine the effect of miR-221 and miR-222 in B cells. Mice bearing either flox or Δ allele(s) exhibited normal B cell development in the bone marrow, with similar numbers and frequencies of pro-B, pre-B, immature, and mature B cells (Fig. 2, A and B). There was a subtle decrease in the frequency of transitional B cell subsets T2 and T3 in the spleens of Δ mice, but there was no difference in the numbers of transitional and mature B cells in the spleen (Fig. 2, C and D). The abundance of serum IgM, IgG1, IgG2b, and IgG3 was unchanged in flox and Δ mice (Fig. 2 E), whereas IgE was below the limit of detection in these unimmunized animals (data not shown). We conclude that the absence of miR-221 and miR-222 does not grossly perturb B cell development in the bone marrow or maturation in the periphery.

miR-221/222 regulate CSR to IgG1 and IgE

To test whether endogenous miR-221/222 regulate CSR, we compared flox and Δ B cells cultured under the same conditions used to screen for functional miRNAs in Dgcr8-deficient B cells. Compared with flox B cells, Δ B cells transfected with an miRNA CM showed a twofold reduction in CSR to IgG1 (Fig. 3 A, compare gray and black bars labeled CM). Transfecting Δ B cells with either miR-221-3p or miR-222-3p mimic restored IgG1 CSR to the frequency seen in CM-transfected flox B cells (Fig. 3 A, compare black bars). These data indicate that the CSR defect in Δ B cells can be reversed by restoring miR-222-3p or miR-221-3p in mature B cells. Furthermore, miR-221-3p or miR-222-3p mimic transfection further increased IgG1 CSR in flox B cells (Fig. 3 A, compare gray bars), indicating that endogenous miR-221/222 is a dose-limited factor that enhances CSR to IgG1.

To determine the expression profile of these miRNAs, we performed quantitative PCR (qPCR) for miR-221-3p and miR-222-3p on RNA from B cells stimulated under various conditions known to induce CSR to IgG1 and IgE where B cells were exposed to LPS + IL-4, anti-CD40 + IL-4, or anti-CD40 + IL-4 + IL-21 for 4 consecutive days. Compared with naive B cells, stimulation with LPS + IL-4 for 4 d increased expression of miR-221-3p and miR-222-3p by 3.7- and 2.5-fold, respectively (Fig. 3 B). Stimulation with anti-CD40 + IL-4 increased miR-221-3p and miR-222-3p expression 8.1- and 3.1-fold, respectively, and the further addition of IL-21 in these conditions increased miR-221-3p induction to 12.5-fold and miR-222-3p to 4.7-fold that of naive cells (Fig. 3 B).

Stimulating flox and Δ B cells with anti-CD40 + IL-4 + IL-21 revealed a requirement for miR-221/222 for optimal CSR to IgG1 and IgE after a 4-d period (Fig. 3, C and D). The frequency of IgE+ cells was significantly reduced in Δ B cells compared with flox B cells in three independent experiments. The frequency of IgG1+ cells was consistently reduced in two of these experiments, with the third showing the highest frequency of IgE+ cells. This could be due to depletion of IgG1+ cells by consecutive CSR to IgE (Cameron et al., 2003; Mandler et al., 1993; Yoshida et al., 1990) or to a higher rate of direct CSR to IgE in this experiment. In any case, comparing the combined frequency of IgE+ and IgG1+ cells revealed a modest and statistically significant CSR defect in Δ B cells compared with flox B cells (Fig. 3 D). Given that CSR correlates with proliferation capacity (Hodgkin et al., 1996),
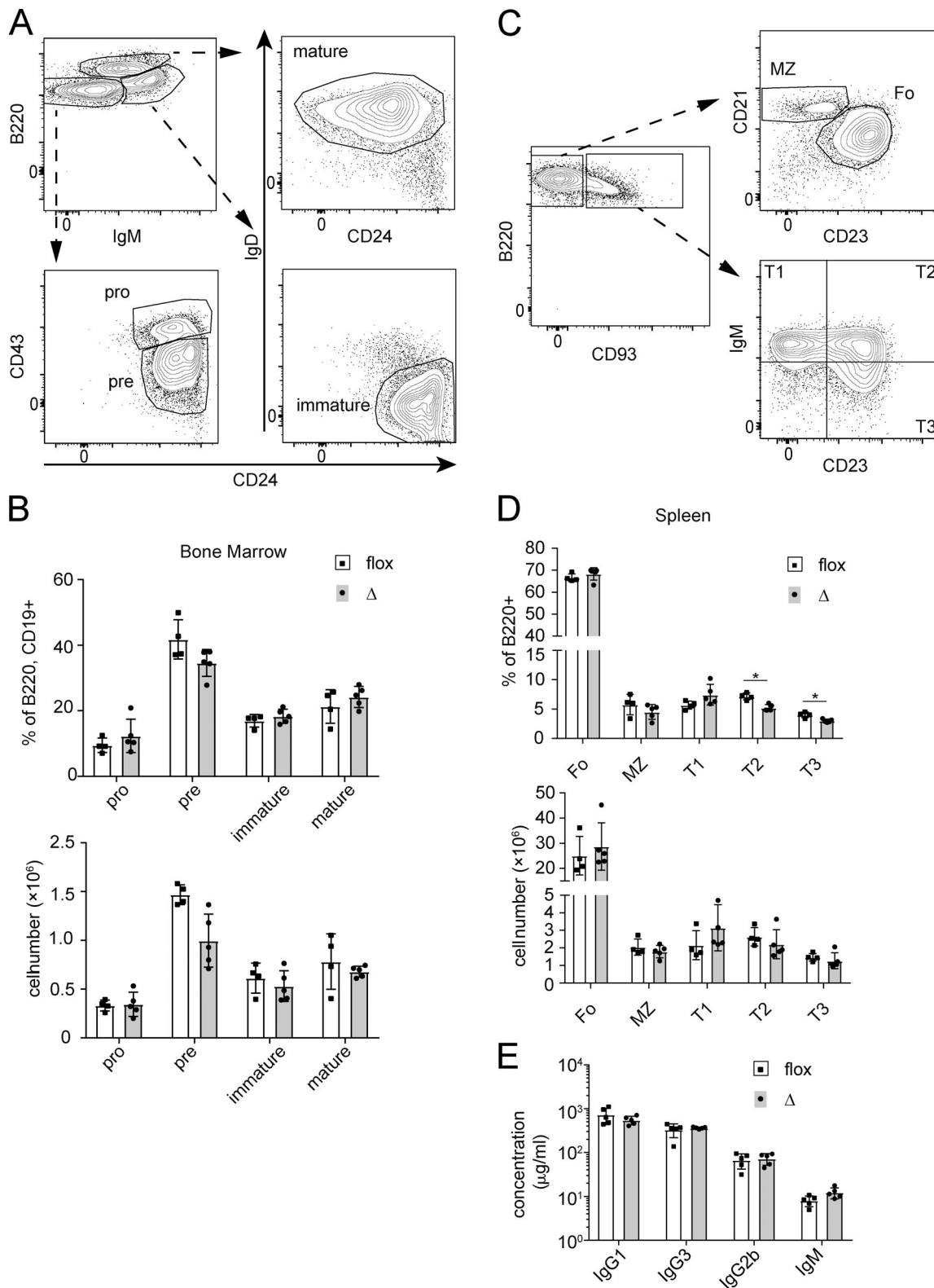
Figure 2. Loss of miR-221/222 does not alter B cell development in the bone marrow or spleen, and steady-state serum antibody levels are unaffected. (A) Representative flow cytometry gating strategy for bone marrow analysis. Upper left gate is a subgate of live, singlet, CD19+, B220+ cells. Further subsetting by B220int, CD43+, CD24+, IgM− pro-B cells; B220int, CD43int, CD24+, IgM− pre-B cells; B220int, CD24+, IgMhi, IgD− immature B cells; and B220hi, IgMint, IgD+, CD24lo mature cells. **(B)** Enumeration of percentage and number of each developmental bone marrow subset determined in A. **(C)** Representative flow cytometry gating strategy for splenic analysis. Leftmost plot is pregated on live, singlet, B220+, CD4− cells that are subdivided into transitional CD93+ subsets CD23−, IgMhi T1; CD23+, IgMhi T2; and CD23+, IgMlo T3 or into mature CD93− subsets CD23+, CD21int follicular and CD23lo, CD21hi marginal zone B cells. **(D)** Enumeration of percentage and number of each developmental splenic subset determined in C. **(E)** Steady-state serum concentrations for the labeled isotypes in flox and Δ mice. All P values were derived from a two-tailed Student's *t* test; P > 0.05 for all unlabeled comparisons; *, P < 0.05. Representative experimental data of two independent experiments with at least four mice per genotype.

Figure 3. **Loss of miR-221/222 leads to defects in B cell CSR to IgG1/IgE in vitro and IgE production in vivo. (A)** Δ or flox B cells were stimulated i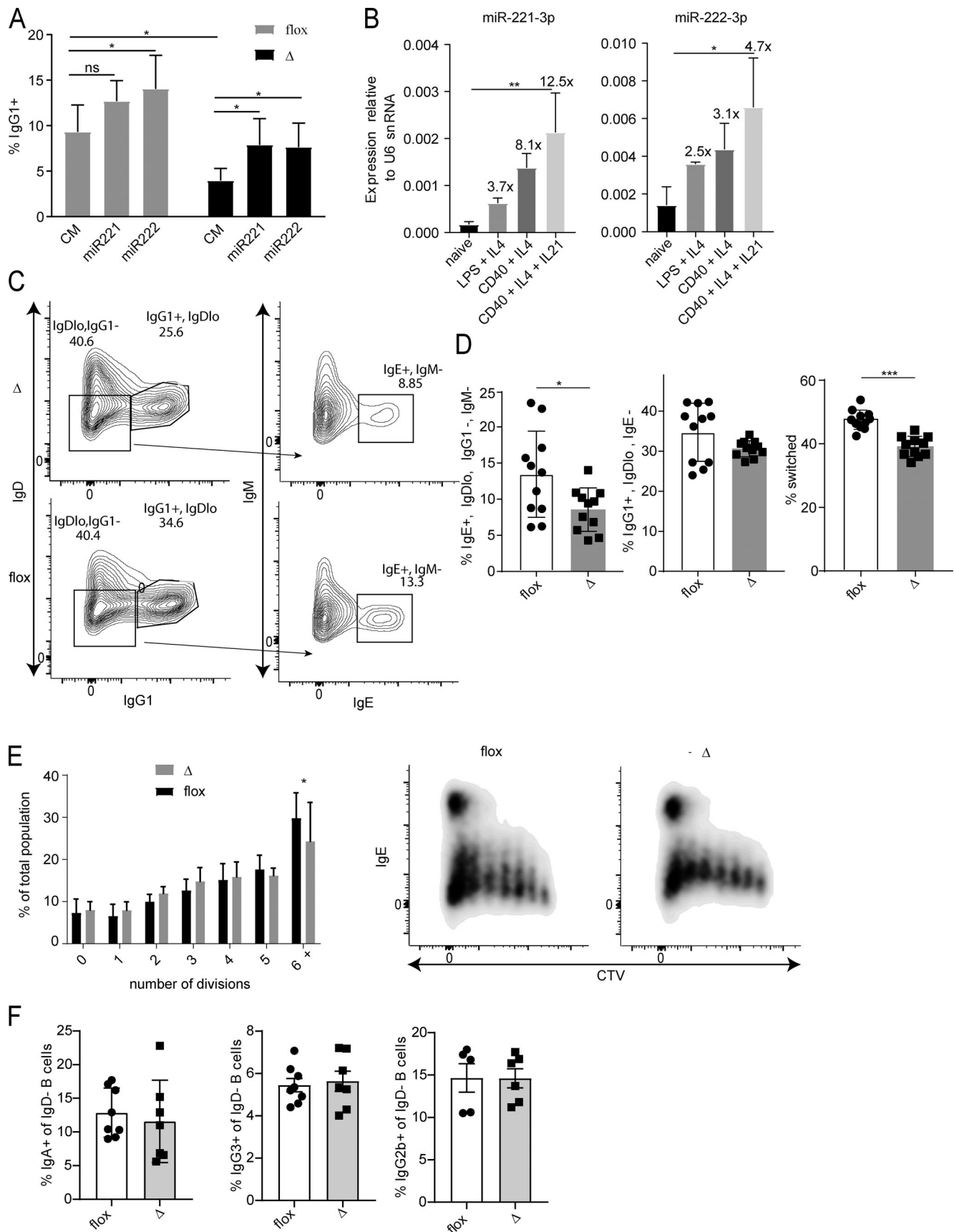dentically to Fig. 1 A and transfected with miR-221-3p (miR-221) or miR-222-3p (miR-222) or CM at day 0, and surface IgG1 was analyzed at day 2. Four mice

per genotype were used, where each mouse was transfected with each mimic. Statistical analysis was performed by repeated measures one-way ANOVA with Dunnett's post-test within each genotype. A representative experiment of three independent experiments is shown. **(B)** Expression of each miRNA relative to U6 small nucleolar RNA (snRNA) in WT C57BL/6 mouse B cells stimulated for 96 h. Data are the average of four biological replicates. Statistical analysis was performed by one-way ANOVA with Dunnett's post-test. **(C)** Representative flow cytometry plots. CSR phenotype of Δ or flox B cells stimulated in anti-CD40 + IL-4 + IL-21 media for 96 h gated on live singlets to determine IgD^{lo}, IgG1$^+$ cells. IgE$^+$ cells are IgM$^-$ and gated from an IgD^{lo}, IgG1$^-$ population. **(D)** Quantification of the percentage of surface IgE$^+$, IgG1$^+$, or either IgG1$^+$/IgE$^+$ from C. A combined three independent experiments with at least three mice per genotype are shown. **(E)** Quantification of division number from cocultured Δ and flox B cells stimulated in anti-CD40 + IL-4 + IL-21 media for 96 h. A paired Student's t test was used for each cocultured well. Combined from three independent experiments with at least two independent cocultures per experiment. CTV, CellTrace Violet. **(F)** CSR phenotype of Δ or flox B cells stimulated for 96 h in CSR conditions to induce IgG3, LPS alone; IgG2b, LPS + TGFβ1; or IgA, anti-CD40 + IL-5 + TGFβ1 + retinoic acid (with or without a proliferation-inducing ligand). *, $P < 0.05$; **, $P < 0.01$; ***, $P < 0.001$.

CellTrace Violet staining was performed on congenically labeled cocultured Δ and flox cells in anti-CD40 + IL-4 + IL-21 conditions to determine if there was a proliferation defect in the absence of these miRNAs. Interestingly, we found that Δ B cells showed a defect in the frequency of cells dividing six or more times compared with flox (Fig. 3 E), indicating a subtle proliferation defect that could influence the frequency of CSR to IgE cells.

To test for defects in CSR to other isotypes in vitro, we stimulated splenic B cells in conditions that induce switching to IgG3, IgG2b, or IgA (Fig. 3 F; Deenick et al., 1999; Seo et al., 2013). Treatment with anti-CD40 + TGFβ1 + IL-5 + retinoic acid induced IgA expression in 12.5% of flox and 12% of Δ B cells. LPS alone induced IgG3 expression in 5% of both flox and Δ B cells, and addition of TGFβ1 induced CSR to IgG2b in 15% of B cells of both genotypes. These data indicate that miR-221/222 regulation of CSR bears some specificity for IgG1 and particularly IgE.

To test whether miR-221/222 expression in B cells influences antibody isotype production in a T cell–dependent response in vivo, we immunized mice with nitrophenyl-conjugated OVA (NP-OVA) adsorbed to alum and measured NP-specific serum antibodies 14 d later. No major differences were observed in the production of antigen-specific IgG1, IgG2b, IgG2c, or IgG3 (Fig. 4 A).

miR-221/222 regulate IgE production in vivo
Having defined a CSR defect in Δ B cells in vitro, we tested whether this defect would translate to a physiological in vivo model of allergy and asthma, specifically house dust mite (HDM) challenge. Examining total IgE titers in mice challenged with HDM revealed a subtle and specific defect in IgE production in Δ mice (Fig. 4 B). IgG1 production was unchanged in this model. We further tested the generation of IgE-expressing plasma cells using a goat anti-IgD polyclonal B cell activation model (Finkelman et al., 1987). At 7 d after immunization, goat anti-IgD serum induced a massive B cell response, with about half of total LN cells composed of CD138$^+$CD19^{int} plasma cells (Fig. 4 C). Although the frequency of total plasma cells was not statistically different between flox and Δ animals (Fig. 4 D), there was a slight defect in this cell population. The frequency of IgE$^+$ plasma cells was decreased in Δ animals compared with flox (Fig. 4 E), as were the total number of plasma cells (Fig. 4 F) and the number of IgE$^+$ plasma cells (Fig. 4 G). This decrease in frequency and number of IgE producers in Δ animals is consistent with the decreased IgE serum levels in HDM-challenged Δ animals and provides a second independent in vivo system in which IgE production is diminished in the absence of miR-221/222-3p.

Combination of Ago2-HITS-CLIP and mRNA sequencing (mRNA-seq) reveals 70 plausible miR-221/222 targets
Having determined the in vitro and in vivo phenotype of miR-221/222-3p in CSR to IgE, we wanted to determine the direct targets of this miRNA family in activated B cells. To determine direct targets of miR-221-3p and miR-222-3p, we performed Ago2-HITS-CLIP on Δ and flox B cells stimulated for 4 d with anti-CD40 + IL-4 + IL-21. This technique captures both miRNAs and their target RNA species bound to the RISC complex protein Ago2, and direct miRNA targets can be determined by comparing miRNA KO and WT cell populations. Libraries were generated and sequenced as previously described (Chi et al., 2009; Gagnon et al., 2019; Loeb et al., 2012). Four independent libraries were generated for Δ and flox genotypes. Analysis of the target transcript space identified the 3′ UTR as the most abundant RNA species target as would be expected, although binding was seen in exon, intron, and 5′ UTR space as well (Fig. 5 A). miRNA sequences were the most abundant RNA species captured (2:1 to 3:1 miRNA/non-miRNA ratio; Fig. 5 B). This indicates either preferential cross-linking of miRNA in Ago2–miRNA–target RNA complexes or an abundance of Ago2–miRNA complexes not yet bound to target RNA sequences in our activated B cells. As expected, both miR-221-3p and miR-222-3p (as well as their star sequence -5p counterparts) were readily captured in flox libraries and essentially absent in Δ libraries, indicating complete deletion of the miRNA genes (Fig. 5 C). This analysis also confirmed that global miRNA expression and loading into Ago2 was not altered in the absence of this miR-221 and miR-222 (Fig. 5 C).

The four Ago2-HITS-CLIP libraries for each genotype were combined for a single comparison of differential peak binding using dCLIP (Wang et al., 2014). Using sequence homology identity of all miR-221/222-3p target sites within the mouse genome identified 10,638 possible binding sites in the annotated 3′ UTRs of the mouse genome. To validate the efficacy in which dCLIP positively identified miR-221/222-3p peaks, differential peaks containing at least a 6-mer target site were binned, and those more bound in the flox than Δ and vice versa were analyzed at increasing differentials determined by the program. Using the internal dCLIP differential ranking metric of at least 1 yielded a total of 652 peaks in 534 gene transcript 3′ UTRs that were more bound in the flox than in the Δ library. However, using the same parameters of a differential of at least 1 yielded a total of 636 peaks in 547 gene transcript 3′ UTRs that were more bound in the Δ than in the flox library, of which 80 of those transcripts overlapped with those in the flox (Fig. S2 A). To improve confidence of the truly differential targets and limit the
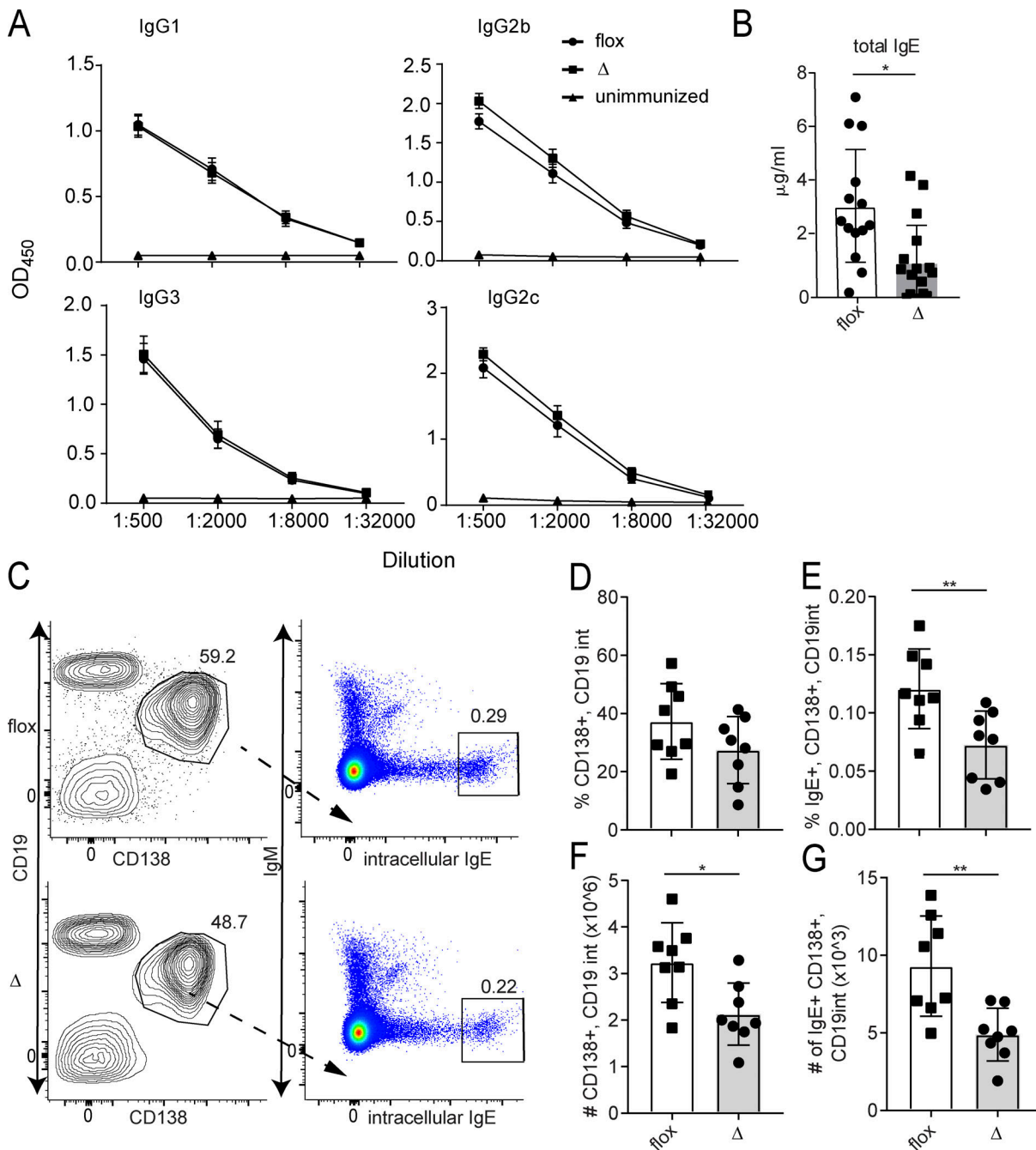
Figure 4. **Loss of miR-221/222 decreases the number of plasma cells (PCs) and IgE⁺ PCs in a pan–B cell activation model of goat anti-IgD immunization. (A)** OD plots for NP-specific isotype antibodies measured in serum 14 d after immunization with NP-OVA in alum. Data are from three independent immunizations with at least four mice per genotype. **(B)** ELISA data for total IgE in mice challenged with HDM for a 2-wk protocol from three independent experiments with at least four mice per group. **(C)** Representative flow plot of the LN cell environment showing PC (CD19int, CD138⁺) gated on intracellular IgE⁺ fraction. **(D)** Frequency of PCs (CD19int, CD138⁺ cells of living singlet). **(E)** Frequency of IgE⁺ PCs. **(F)** Numbers of PCs. **(G)** Numbers of IgE⁺ PCs. A combination of two independent experiments with at least four mice per genotype per experiment is shown. All statistics are from a two-tailed Student's *t* test. *, P < 0.05; **, P < 0.01.

amount of seed sites that were more occupied in Δ and flox due to spurious read differences from adjacent miRNA binding, a differential of 10 was used, and, in this case, at least 6-mer containing peaks more bound in the flox led to a total of 412 peaks in 343 gene transcript 3′ UTRs. When the analysis was performed with the differential of 10 on sites more bound in Δ

libraries than in flox libraries, only 61 peaks were found in 57 gene transcript 3′ UTRs, and of these, only 8 gene transcripts overlapped with those of flox (Fig. S2 B).

RNA-seq was performed on flox and Δ B cells stimulated similarly to the Ago2-HITS-CLIP libraries to determine differentially expressed genes between Δ and flox activated B cells. A
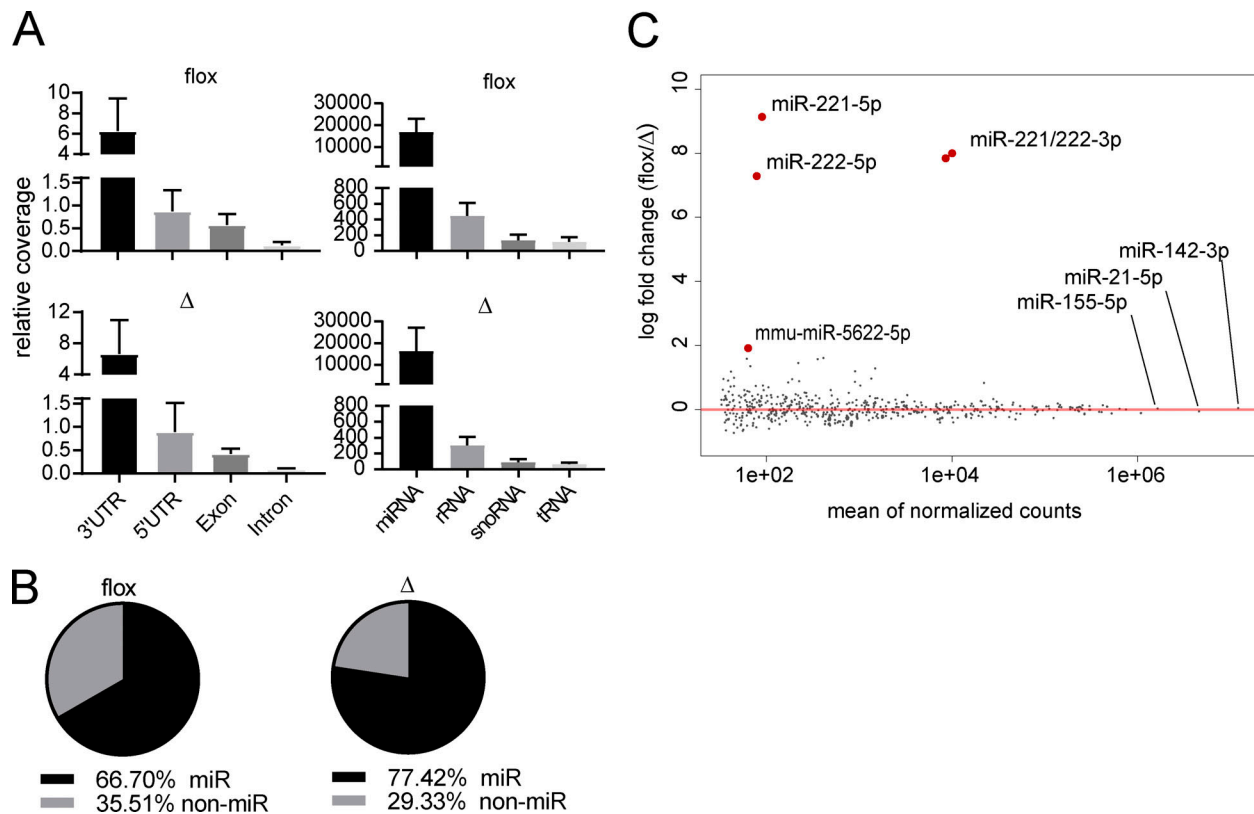
Figure 5. **Characterization of Ago2 binding in Δ or flox B cells stimulated with anti-CD40, IL-4, IL-21. (A)** Annotations and relative coverage of reads from each of the Δ and flox B cell libraries aligning to annotated mRNA sequences (left) and noncoding RNA sequences (right) averaged from four libraries for each genotype. snoRNA, small nucleolar RNA. **(B)** Distribution of miRNA and non-miRNA reads in each library. **(C)** Mean analysis plot for miRNA reads only. Mean miRNA read count versus $\log_{10}$ miRNA read count per million of flox versus Δ reads. Red dots are differentially captured miRNAs by DESeq2 with false discovery rate <0.05.

total of 12,074 Ensembl transcripts were found to be expressed under these conditions, of which 429 were differentially expressed by a false discovery rate < 0.1. Of these differentially expressed transcripts, 286 were up-regulated in the KO compared with the flox libraries. The 12,074 transcripts were binned into subsets containing no miR-221/222-3p seed match, only 6-mer match, at least 7-mer match (+ 6-mer), or at least 8-mer match (+ 7-mer + 6-mer) binding sites in annotated 3′ UTRs. Cumulative distribution function (CDF) plots were generated, and each seed-containing bin was compared with the no seed bin generating a differential D = 0.132 for 6-mer, D = 0.126 for 7-mer, and D = 0.171 for 8-mer, indicating increased differential expression of 8-mer seed match–containing transcripts in the Δ compared with flox B cells (Fig. 6 A). The absence of miR-221/222 leads to a subtle increase in expression of all genes containing a putative seed sequence by sequence match alone. Using these 343 dCLIP putative target genes to create a CDF plot compared with all other expressed genes led to a differential of D = 0.19 (Fig. 6 B), indicating an increased confidence of these genes being direct targets and providing more confidence of direct targeted regulation by miR-221/222-3p than that of putative seed sequence match alone.

To compare our dCLIP analysis with predicted targets from the sequence homology, we analyzed the predicted target genes from the Bartel laboratory's TargetScan 7.1 program (Agarwal et al., 2015). TargetScan 7.1 predicts 404 gene targets for the

miR-221/222-3p family, of which 290 were expressed in our B cell cultures by RNA-seq. Generating CDF plots of the 290 TargetScan predicted genes compared with all others produced a differential D = 0.193 (Fig. 6 C), further increasing the confidence of these genes being directly targeted by miR-221/222-3p. Of these 290 TargetScan predicted gene targets, 70 of them overlapped with those 343 gene targets predicted from our differential HITS-CLIP analysis (Fig. S2 C). Creating a further CDF plot comparing these 70 putative targets with all other genes further increased the differential D = 0.293, providing strong confidence for these genes being directly regulated by this miRNA family (Fig. 6 D). The union of both cell-specific dCLIP and the predictive capabilities of TargetScan 7.1 provided a subset of genes we could directly test through small inhibitory RNA screening. Running Metascape (Zhou et al., 2019) on the 70 genes provided a gene ontology profile enriched in a cell cycle profile, among others (Fig. 6 E), congruent with our finding of this miRNA regulating proliferation in mature B cells and findings in other cell types (Galardi et al., 2007; Mayoral et al., 2009).

siRNA screen of the 70 direct gene targets implicates Foxp1, cd164, and Arid1a as regulators of CSR to IgG1/IgE

To interrogate the putative targets as potential regulators of CSR, we performed an siRNA screen similar to the miRNA
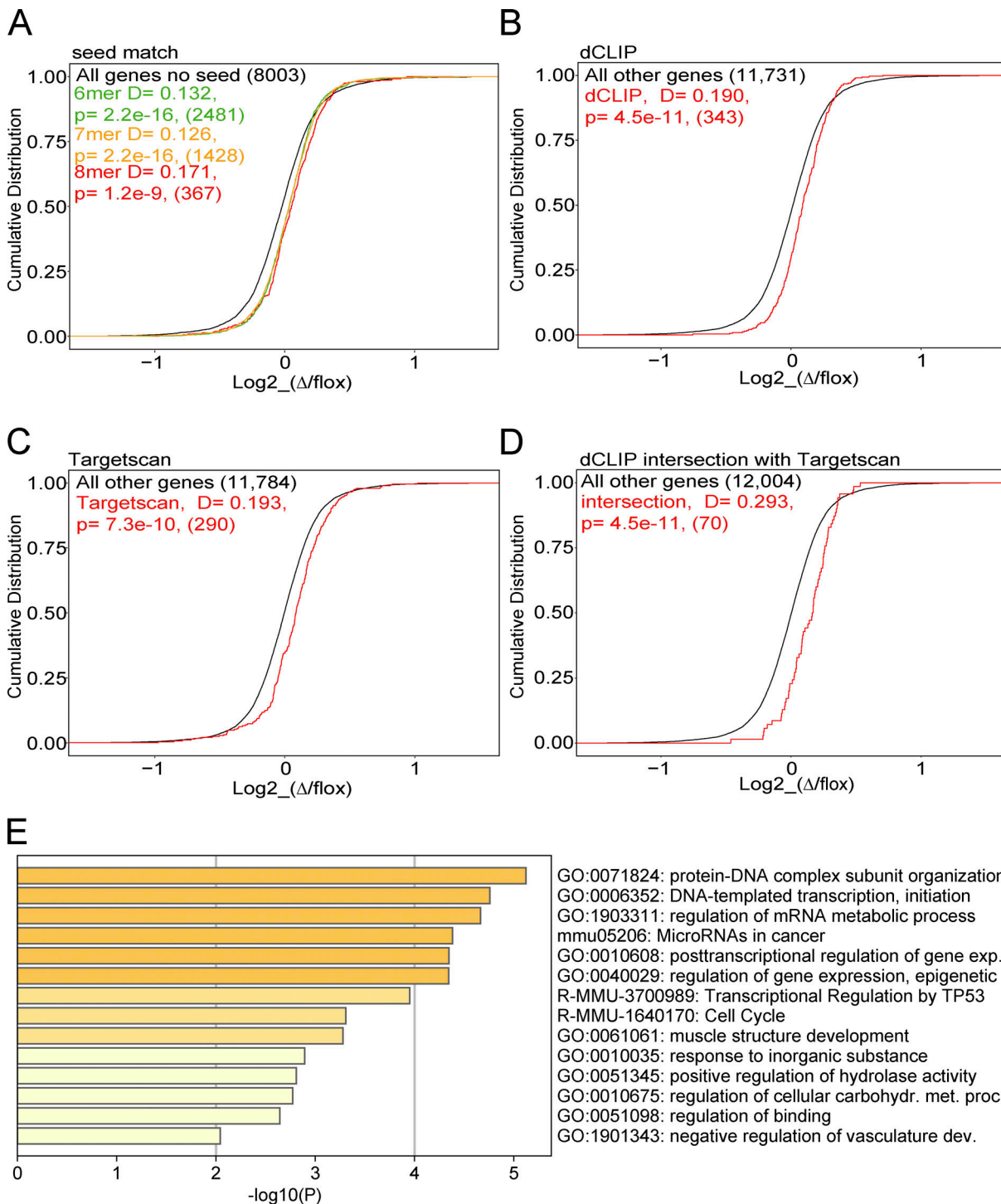
Figure 6. Intersection of dCLIP, RNA-seq, and TargetScan indicates 70 possible gene targets of miR-221/222 in B cells. (A–D) CDF plots comparing RNA-seq gene expression on x axis versus cumulative distribution on y axis. **(A)** Genes with at least one 6-mer (green), at least one 7-mer (orange), or at least one 8-mer (red) compared with those lacking an miR-221/222-3p seed site (black). **(B)** dCLIP predicted genes (red) compared with all others (black). **(C)** TargetScan predicted genes (red) compared with all others (black). **(D)** dCLIP and TargetScan predicted genes (red) compared with all others (black). **(E)** Ranked gene ontology (GO) terms and Kyoto Encyclopedia of Genes and Genomes pathways enriched in the dCLIP and TargetScan gene subset.

screen depicted in Fig. 1. B cells from WT mice were first activated in anti-CD180 + low-dose IL-4 and then transferred to canonical CSR conditions of LPS + high-dose IL-4. Four siRNAs were used per gene target, and surface IgG1^{+} and viability were analyzed by flow cytometry. Of the 70 targets, siRNA

knockdown (KD) of the pro-apoptotic factor *Bcl2l1* (Bim protein) increased viability of transfected cells to 65%, a 15% increase from control siRNA (Fig. 7 A). Furthermore, siRNA KD of *Rnps1*, an enzyme necessary for pre-mRNA splice junction formation (Mayeda et al., 1999), negatively regulated both CSR

to IgG1 and viability. siRNA KD of three candidate miR-221/222 targets, *Foxp1*, *Cd164*, and *Arid1a*, resulted in the highest increases of surface IgG1 frequency compared with control siRNA (Fig. 7 A). This increase of IgG1 frequency was confirmed in an siRNA rescreen where KD of these three targets resulted in the highest frequency of IgG1⁺ B cells (Fig. 7 B). *Foxp1* and *Arid1a* expression was significantly higher in Δ mice than in flox mice (1.45- and 1.40-fold increased, respectively), whereas *Cd164* expression was only moderately different between the two genotypes at 1.06-fold higher in Δ versus flox mice (Fig. 7 C). We constructed dual luciferase reporter constructs to test whether these transcripts' 3′ UTRs were directly responsive to miR-221/222. Both *Cd164* and *Foxp1* 3′ UTR fragments containing the TargetScan 7.1 predicted binding sites (as well as an additional 6-mer miR-221/222 binding sequence in the 3′ UTR of *Foxp1*) showed decreased activity in the presence of miR-221/222. Although we did not detect significant effects with our *Arid1a* 3′ UTR construct, previous studies have demonstrated direct targeting by miR-221/222 using similar assays in other cells (Shi et al., 2019; Yang et al., 2016). These findings, in conjunction with differential binding detected by Ago2-HITS-CLIP, support the conclusion that *Cd164*, *Arid1a*, and *Foxp1* are direct targets of miR-221/222.

Genetic ablation of Foxp1 increases B cell propensity to switch to IgG1 and IgE

To confirm that Foxp1 modulates CSR to IgG1 and IgE, we used a tamoxifen-inducible Cre deletion model of *Foxp1* and then cultured the cells under IgG1/IgE class-switching conditions (Fig. 8 A). Foxp1-deleted (Foxp1-KO) follicular B cells cultured on B cell activating factor (BAFF)/CD40L-expressing cells in the presence of IL-4 showed a threefold increase in the frequency of IgG1 and IgE surface expression compared with Foxp1^fl/fl^ or Cre^ERT2^ (Foxp1-WT) cells (Fig. 8 B). Induction of CSR to IgG1 ranged from 10% to 60% from experiment to experiment, whereas that of IgE ranged from 3% to 20%. However, there was a consistent 2.5–3-fold higher induction of IgG1 and IgE isotype switch in Foxp1-KO B cells than in Foxp1-WT B cells (Fig. 8 C). As expected, CSR to both IgE and IgG1 required IL-4, indicating that the activated B cells were not switching during tamoxifen treatment in the in vivo setting. This confirmation of the siRNA KD implicates miR-221/222–mediated *Foxp1* regulation as a modulator that influences CSR to IgG1 and IgE in B cells.

Genetic ablation and chemical inhibition of Arid1a affects IgG1 and IgE CSR

We used a genetic approach to limit *Arid1a* expression in B cells, crossing CD21^Cre^ (Cre+WT) and *Arid1a*^fl/+^ (Arid1a-WT) mice to generate CD21^Cre^*Arid1a*^fl/+^ (Arid1a-HET) mice with B cells carrying only one functional Arid1a allele. Cre-mediated heterozygosity decreases *Arid1a* transcript and protein levels (Gao et al., 2008). Complete deletion of Arid1a in the hematopoietic system causes profound defects in development (Han et al., 2019), but Arid1a-HET B cells developed normally. Stimulation in IgE CSR conditions (anti-CD40⁺IL-4⁺IL-21) in vitro induced lower frequencies of IgE-expressing cells among Arid1a-HET B cells than Cre+WT and Arid1a-WT controls (Fig. 9 A, right panel), although

there was an increase in the frequency of IgG1⁺ B cells (Fig. 9 A, left panel). These results indicate that partial genetic loss of this BAF complex member alters CSR fate in these conditions.

We also used a specific Arid1a–BAF complex chemical inhibitor, the macrolactam BRD-K80443127, to test the effect of BAF complex dysregulation on CSR to IgG1/IgE. Cells cultured in IgE CSR conditions (anti-CD40⁺IL-4⁺IL-21) showed no decrease in viability in the presence of BRD-K80443127 (Fig. 9 B, top left panel) and even a slight increase at the 20–40 μM range, indicating that dysregulation of these complexes is not vital for mature B cell survival under this stimulus. Similarly, plasma cell differentiation showed a defect only at the highest concentration of 40 μM (Fig. 9 B, top right panel). In contrast, both IgG1 and IgE CSR exhibited a dose-dependent decrease (Fig. 9 B, bottom left and bottom right, respectively). Consistent with the results in Arid1a-HET B cells, IgE CSR was particularly sensitive to Arid1a-BAF inhibition, with dose-sensitive significant effects beginning at 5 μM. IgG1 frequency was reduced to 80% of vehicle control at 10 μM of BRD-K80443127 and fell off sharply at 40 μM, a concentration that also affected plasma cell differentiation. Targeting Arid1a through both genetic and chemical means revealed that this miR-221/222-3p–regulated gene modulates CSR to IgG1 and especially IgE.

Discussion

miRNA rescue screens have been used to study embryonic stem cell pluripotency and self-renewal (Froidure et al., 2016; Wang et al., 2008) and in miRNA-depleted lymphocytes to study T cell proliferation, differentiation, and cytokine production (Pua et al., 2016; Steiner et al., 2011). In this study, we developed and executed a rescue screen in primary mouse B cells to reveal that miR-221/222 can positively regulate CSR to IgG1, and we leveraged this finding to elucidate a previously unknown miRNA-regulated gene network that modulates CSR to IgG1 and IgE. These rescue screens measure the effects of individual miRNAs introduced at potentially supraphysiological quantities in the absence of other miRNAs. However, analysis of miR-221/222–deficient B cells demonstrated that endogenous miR-221/222 regulate CSR in vitro and in vivo. Extending this screen for miRNA influence with biochemical elucidation of direct targets of miR-221/222, we uncovered evidence for a network of downstream regulators of CSR, including *Foxp1*, *Arid1a*, and *Cd164*.

Our investigation of miR-221/222 and its targets uncovered the role of *Foxp1* as a negative regulator of CSR to IgE. *Foxp1* is essential for B cell development (Hu et al., 2006), and its downregulation in activated mature B cells is necessary for germinal center entry and plasma cell differentiation (Sagardoy et al., 2013; van Keimpema et al., 2015). *Foxp1* overexpression decreases CSR to IgG1 in both mouse and human B cells (Sagardoy et al., 2013), congruent with our findings of increased CSR to IgG1 in *Foxp1*-deficient B cells and opposing decreases in CSR and increased *Foxp1* expression in miR-221/222–deficient B cells. Similarly, the reduced plasma cell generation we observed in cultured miR-221/222–deficient B cells may be related to increased expression of *Foxp1*, whose overexpression interferes
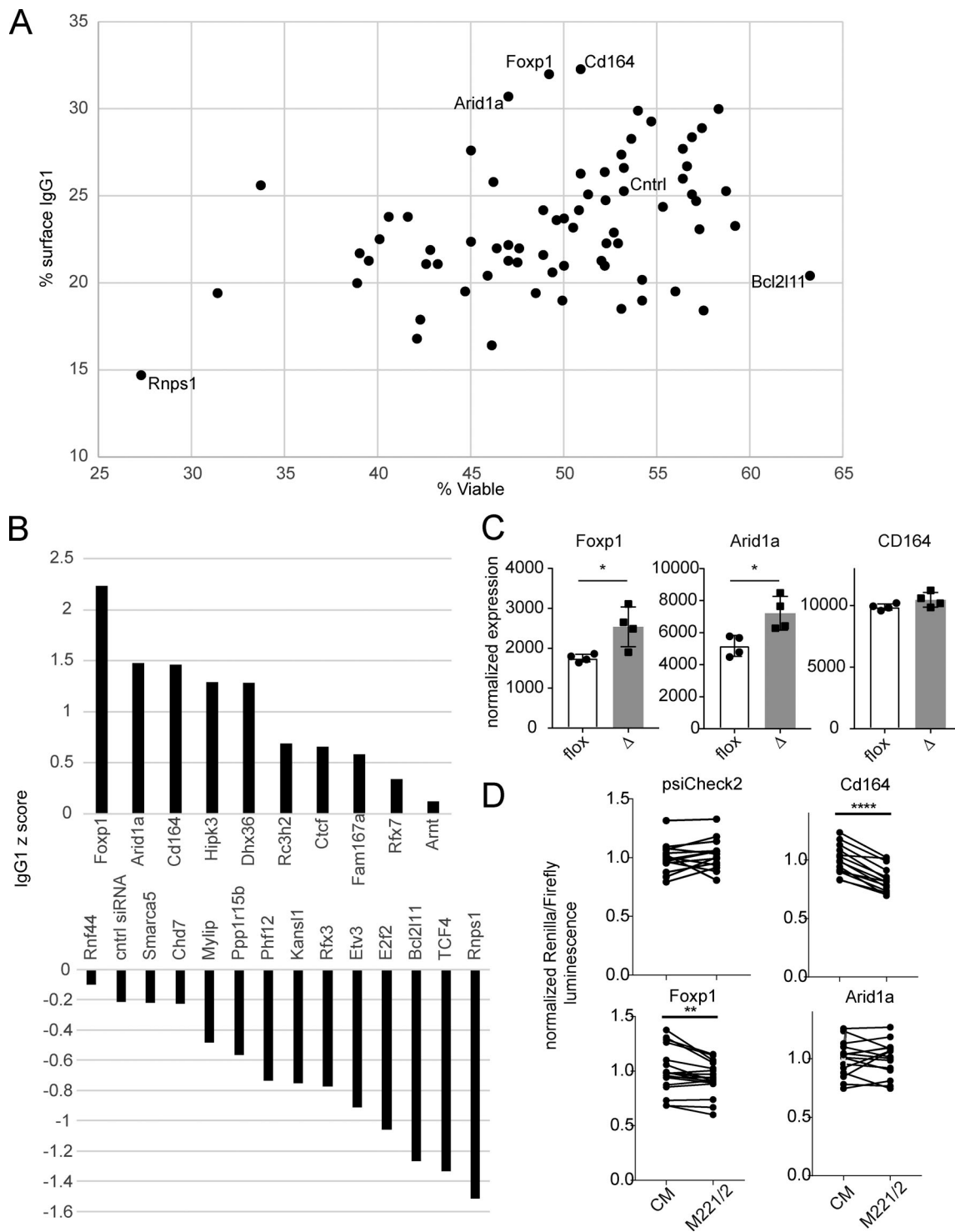
Figure 7. **siRNA KD screen on dCLIP and TargetScan predicted miR-221/222-3p gene targets identifies Foxp1, Arid1a, and CD164 as regulators of CSR.**
(A) Frequency of viable versus frequency of surface IgG1⁺ for the siRNA KD of 70 gene targets predicted by dCLIP and TargetScan from a single screen on B cells pooled from four Δ mice stimulated and analyzed exactly as in the Fig. 1 miRNA screen. **(B)** Z-score plot for surface IgG1 for a rescreen of the top 10 and bottom 10 genes from A. **(C)** Gene expression data for *Foxp1*, *Arid1a*, and *Cd164* from RNA-seq data. **(D)** Dual luciferase reporter assay results for Δ B cells transfected with either CM or miR-221/222-3p mimic and labeled psiCHECK-2 constructs containing >1 kb of each annotated 3′ UTR containing the miR-221/222 target sequence. Combined data from three to five independent experiments where each connected data point represents the average of four technical replicates normalized to CM luciferase mean within each experiment. *, P < 0.05; **, P < 0.01; ****, P < 0.0001.
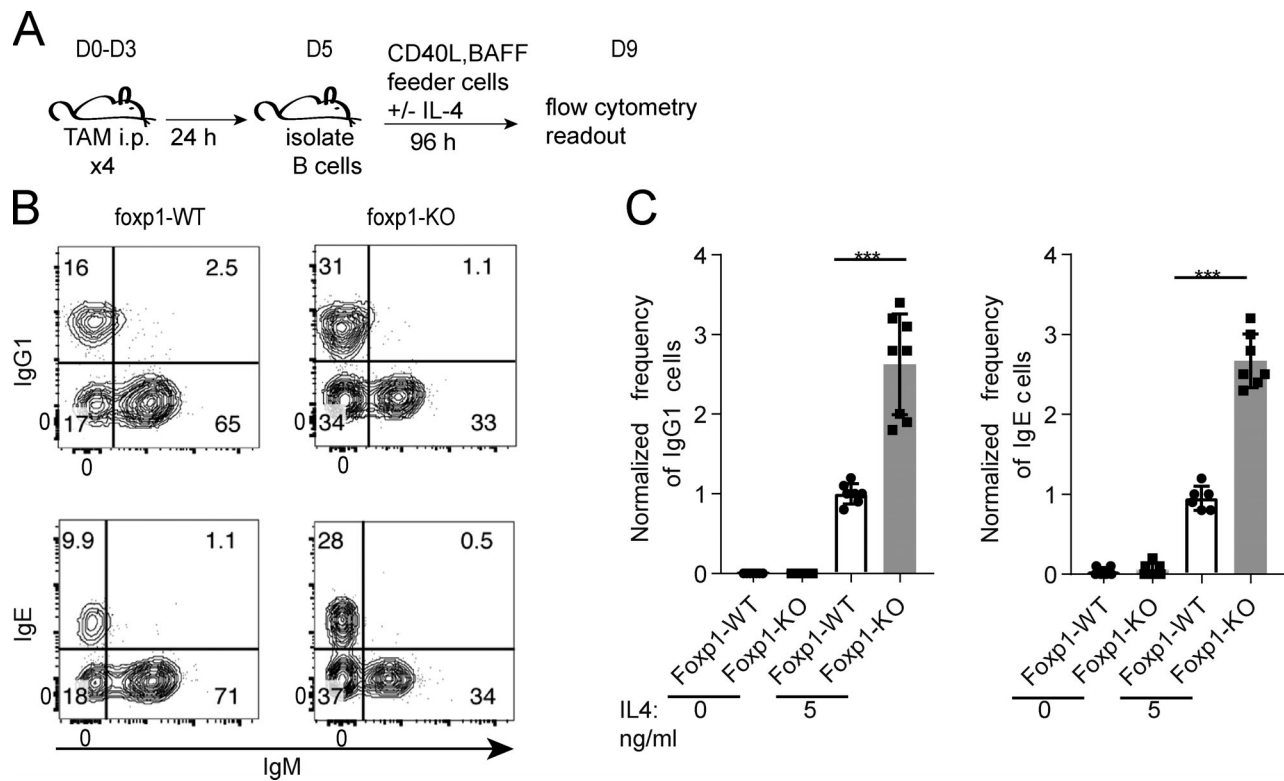
Figure 8. **Genetic ablation of *Foxp1* increases the propensity for activated B cells to switch to IgG1 and IgE. (A)** Schematic for tamoxifen (TAM)-induced deletion and culturing of Foxp1-WT and Foxp1-KO B cells. D0–D3, days 0–3; D5, day 5; D9, day 9. **(B)** Representative flow cytometry plots of B cells from Foxp1-WT and Foxp1-KO mice after stimulation with supplemental IL-4 pregated on live CD19$^+$ singlets. **(C)** Normalized frequency of IgG1 and IgE surface expression. Each data point represents an individual biological replicate pooled from three independent experiments that were normalized to mean WT Ig frequency (of 1) within each experiment. Statistics were generated by two-tailed Student's *t* test. ***, P < 0.001.

with plasma cell generation (van Keimpema et al., 2015). *Foxp1* deletion in mature B cells also hinders T cell–independent B cell responses, production of IgG3, and B1 cell development (Patzelt et al., 2018). A previous study of T cell–dependent antibody responses showed no clear difference in IgG1 serum titers in B cell lineage–specific *Foxp1*-deficient mice (Dekker et al., 2019; Patzelt et al., 2018), but this finding is complicated by developmental defects that result in fewer mature B cells in these mice (Hu et al., 2006). *Foxp1*-deficient B cells did not show proliferative defects in our system, decoupling the CSR defect in these mice from proliferation. Whether FOXP1 acts to dampen activation signals, cell cycle regulators, or other factors remains to be determined. Further studies are needed to fully elucidate the transcriptional targets and downstream mechanisms through which FOXP1 controls CSR in conjunction with its effects on B cell fate decisions.

The role of chromatin architecture and remodeling in the context of CSR has recently come into full appreciation as DNA orientation and chromatin regulation were shown to be critical for switch site orientation and stabilization for AID-mediated mutation (Yu and Lieber, 2019; Zhang et al., 2019). Interestingly, our analysis of regulated miR-221/222 interactors identified three predicted targets that play a role in chromatin remodeling: *Ctcf*, *Smarca5*, and *Arid1a*. CTCF is a central regulator of chromatin domain architecture and CSR (Pérez-García et al., 2017; Thomas-Claudepierre et al., 2013; Zhang et al.,

2019). Human *Ctcf* is an established target of miR-221/222 (Lupini et al., 2013). *Arid1a* encodes a key component of the BAF nucleosome remodeling complexes, which are critical for chromatin remodeling during hematopoiesis (Han et al., 2019). We found that the action of these complexes is necessary for B cell activation because cells cultured with an inhibitor of Arid1a-containing BAF complexes (Marian et al., 2018) remained in a quiescent state, undergoing neither cell death nor proliferation. However, genetically or pharmacologically limiting (rather than eliminating) Arid1a-containing BAF complexes selectively affected CSR, consistently reducing the generation of IgE-expressing cells. B cells with only one functional *Arid1a* allele exhibited a surprisingly specific defect in IgE CSR with increased production of IgG1$^+$ cells, whereas pharmacological inhibition decreased the frequency of both IgE- and IgG1-expressing cells. This discrepancy may be attributable to differences in BAF complex formation because genetically altered B cells with reduced *Arid1a* expression may form more non–Arid1a–BAF complexes that would not be present in acute inhibition experiments. Whether Arid1a–BAF complex nucleosome remodeling mediates access to critical regions of the *Igh* locus deserves further study. In any case, the selective sensitivity of IgE CSR to BAF inhibition indicates the existence of isotype-specific effects of regulating (or dysregulating) this machinery.

Previous studies of miR-221/222 in other immune cell types and cancer demonstrated direct regulation of *Cdkn1b*, which
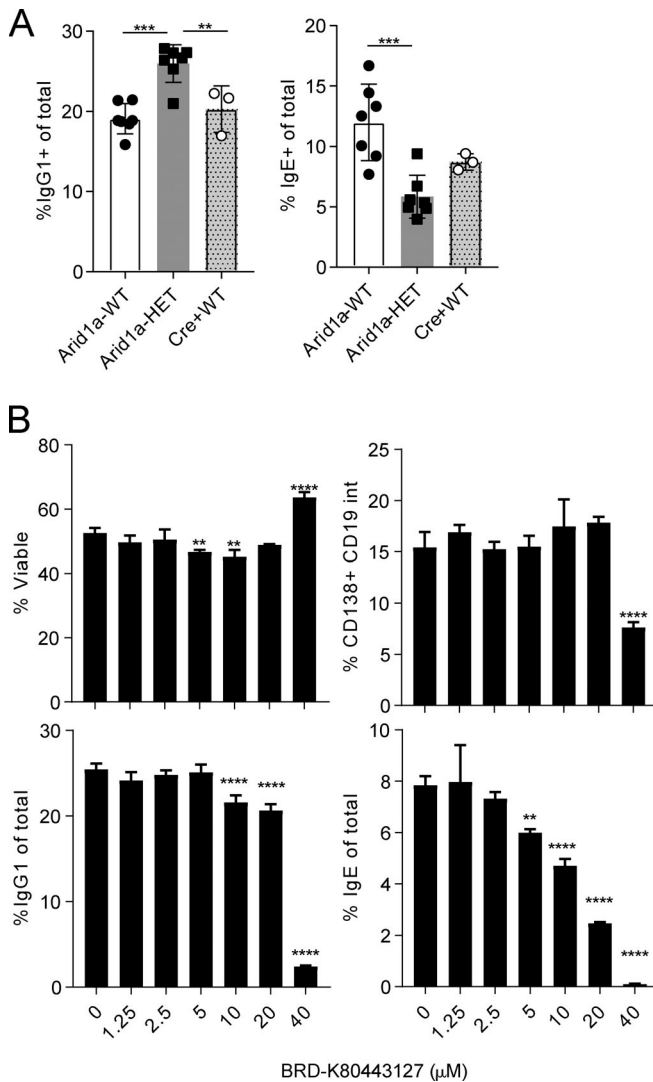
Figure 9. **Genetic ablation of *Arid1a* and chemical inhibition of Arid1a–BAF complexes alters B cell IgG1 and IgE CSR frequency. (A)** Quantification of Arid1a-WT, Arid1a-HET, and Cre+WT B cells stimulated with anti-CD40+IL-4+IL-21 frequency to switch to IgG1 and IgE. Combined data from two independent experiments with at least three mice per genotype are shown. **(B)** Quantification of viability, frequency of plasma cells (CD138+, CD19int), and frequency of IgG1 or IgE surface expression throughout dilution series of chemical lactam. Statistics were generated by one-way ANOVA with Dunnett's multiple comparison test in A for all comparisons with vehicle alone. Leftmost column is a representative experiment of three independent experiments. **, $P < 0.01$; ***, $P < 0.001$; ****, $P < 0.0001$.

encodes p27-kip protein, a positive regulator of cell cycle progression from G_1 to S (Fornari et al., 2008; Galardi et al., 2007; Mayoral et al., 2009). Our biochemical data also implicated *Cdkn1b* as a direct target. However, siRNAs targeting this gene and its effect on cell proliferation had no discernible effect on CSR. Although our data do not definitively prove that miR-221/222 directly target *Cdkn1b* in B cells, the fact that miR-221/222–deficient B cells exhibited a subtle proliferative defect implicates these miRNAs in the regulation of B cell cycle progression, possibly through multiple targets, including *Cdkn1b*. This subtle decrease in proliferation likely contributes to, but is not sufficient

to mechanistically explain, the more robust CSR defect, which appears to be further coordinated by miR-221/222 regulation of epigenetic and transcription factor targets elucidated in this study.

miR-221/222 regulates allergic responses through coordinate control of multiple cell types. Mast cells, basophils, and other granulocytes very strongly express miR-221/222 (Kuchen et al., 2010; Monticelli et al., 2005), and these miRNAs regulate mast cell proliferation and degranulation in response to IgE receptor cross-linking (Mayoral et al., 2011; Mayoral et al., 2009). In this study, we found that miR-221/222 deficiency also impaired B cell production of IgE in allergic airway sensitization and pan–B cell activation models. Further studies will be necessary to determine whether miR-221/222 absence in granulocyte populations further affects allergic responses in vivo. The control of complex immunological processes through regulation of distinct cell types by a common factor is an interesting regulatory phenomenon exemplified by the orchestration of humoral responses by the transcription factor BCL6 (Crotty, 2019; Okada et al., 2012) and the miRNA cluster miR-17~92 (Baumjohann et al., 2013; Jin et al., 2013; Kang et al., 2013) acting in both germinal center B cells and T follicular helper cells.

Other highly expressed miRNAs also regulate humoral immune responses, including miR-155 and miR-181b, both of which directly target the critical CSR factor *Aicda* in B cells (Dorsett et al., 2008; Rodriguez et al., 2007; Teng et al., 2008; Thai et al., 2007; Vigorito et al., 2007; de Yébenes et al., 2008). miRNA expression is dramatically modulated in activated B cells (Fowler et al., 2015; Kuchen et al., 2010). In our experiments, miR-221/222 were up-regulated upon B cell activation; yet, their abundance was still <1% that of the most highly expressed miRNAs. Nevertheless, in comparing Ago2 binding, we observed that gene expression in the presence and absence of miR-221/222 singled out direct targets even for these modestly expressed miRNAs. We provide these data as a resource for mining the Ago2-bound transcript space in mouse B cells activated to mimic T cell–dependent stimulation, complementing previous experiments performed under different conditions (Hsin et al., 2018; Jin et al., 2013).

Unbiased investigation of miR-221/222 target genes identified by Ago2-HITS-CLIP and gene expression analysis revealed a functionally relevant downstream gene network actively regulated in B cells undergoing CSR. Our overall experimental approach, which we term "miRNA-directed target pathway discovery," co-opts the coevolution of miRNAs and their targets to reveal novel players in biological processes without requiring genome-wide functional screens. miRNA-directed pathway discovery can be adapted to interrogate cell type–specific miRNA and target networks operative in nearly any biological process.

Materials and methods
Mice
Mice used in this work included Cγ1-cre, B6.129P2(Cg)-Ighg1tm1(cre)Cgn/J (Casola et al., 2006); CD21-Cre, B6.Cg-Tg(Cr2-cre)3Cgn/J (Kraus et al., 2004); Dgcr8fl/fl, B6.Cg-Dgcr8tm1.1Blel/J (Rao et al., 2009); R26-LSL-YFP, B6.Gt(ROSA)26Sortm1(EYFP)Cos/J (Srinivas et al., 2001); CreERT2, B6.Cg-Ndor1Tg(UBC-cre/ERT2)1Ejb/1J

(Ruzankina et al., 2007); *Foxp1*fl/fl, Foxp1tm1.1Pwt/J (Feng et al., 2010); Arid1afl/fl, 129.Arid1atm1.1Zhwa/J (Gao et al., 2008); and flox: Mirc53fl/y or Δ: Micr53-/y. Only male mice were used for miR-221/222 deletion experiments, although some female mice were used for creating the Ago2-HITS-CLIP libraries. For NP-OVA immunizations and IgG2/IgA in vitro CSR assays, some mice included were Mb1-cre+ fl/y with fl/y controls. For Foxp1 deletion, CreERT2Foxp1fl/fl R26-LSL-YFP mice have been previously described (Feng et al., 2011). For CD21-Cre–mediated Arid1afl/fl genetic deletion experiments, B6.129 N1 Arid1a-HET and Arid1a-WT mice were used, and B6.129N2-HET and Cre+WT mice were also used, all of which were littermate matched. All mice were age and sex matched between 6 and 16 wk for all experiments where littermates were not explicitly used. All mice were cared for and experimented on under the guidance of the University of California, San Francisco, and University of Alabama at Birmingham laboratory animal research centers in compliance with approved institutional animal care and use committee protocols.

B cell isolation, transfection, and stimulation

Splenic naive B cells were isolated using Dynabead untouched B cells (CD43 negative selection kit; Thermo Fisher Scientific) and stimulated in RPMI 1640 medium supplemented with 10% FCS, Hepes, 50 μM 2-ME, and L-glutamine. Pretransfection stimulation consisted of 250 ng/ml anti-CD180 (RP105; Bio-Legend) and 1 ng/ml mIL-4 (PeproTech) at 10^6 cells/ml in 12-well plates at 4 ml per well (Costar) for transfection conditions. After 48 h, cells were washed in 2× PBS and resuspended at 10^5 cells/10 μl in Neon transfection buffer R (Invitrogen) and mixed with siRNA (Dharmacon/GE Healthcare), miRNA mimic (Dharmacon/GE Healthcare), and/or luciferase plasmid before being immediately electroporated for 3 × 10 ms at 1,550 V on a Neon transfection instrument. The 10-μl transfection was then transferred directly into 200 μl of CSR media in a round-bottomed 96-well plate (Costar). For IgG1/IgE CSR conditions, cells were stimulated with 3 μg/ml LPS (from *Salmonella*; Sigma-Aldrich) and 25 ng/ml IL-4 for miRNA and siRNA screens or in 500 ng/ml to 1 μg/ml anti-CD40 (FGK45.1.1; Miltenyi Biotec), 25 ng/ml IL-4, and 10–12.5 ng/ml IL-21 (eBioscience) at 10^5 cells/200 μl/well in a 96-well round-bottomed plate. Other CSR conditions consisted of 10 ug/ml LPS alone for IgG3; 10 μg/ml LPS + 1 ng/ml human TGFβ1 (PeproTech) for IgG2b; and 200–250 ng/ml anti-CD40, 5–10 ng/ml IL-5 (PeproTech), 10 nM retinoic acid, and 1 ng/ml human TGFβ1 with or without 180 ng/ml APRIL (PeproTech) for IgA. For the ARID1A–BAF complex chemical inhibitor assay, cells were stimulated with BRD-K80443127 dissolved in DMSO at the reported concentration or with vehicle alone.

Foxp1 deletion and CD40LB feeder cell stimulation

For Foxp1 deletion, CreERT2Foxp1fl/fl R26-LSL-YFP (Foxp1-KO), CreERT2Foxp1wt/wt R26-LSL-YFP, and/or CreERT2Foxp1wt/wt R26-LSL-YFP (Foxp1-WT) mice were treated i.p. daily for 4 d (days 0–3) with tamoxifen (Sigma-Aldrich) at a dose of 3 mg per mouse and were allowed to "rest" for 1 d (day 4). CD40L-Baff 3T3 feeder cells (Nojima et al., 2011) that were plated at 2 × 10^5 per

well in 24-well culture-treated plates on day 4. Spleens were harvested on day 5, and Foxp1-deficient follicular B cells (CD3⁻, CD19⁺, CD21/35low, CD23⁺, YFP⁺) were FACS sorted and cocultured at 2 × 10^5 B cells/well with precoated CD40L-Baff 3T3 feeder cells with and without IL-4 (R&D Systems) for 4 d (day 9).

RNA isolation, qPCR, and RNA-seq

Stimulated B cells were pelleted, and RNA was extracted using TRIzol reagent (Thermo Fisher Scientific). RNA was extracted using the RNeasy Micro Kit (Qiagen). cDNA was generated with one-step Mir-X (Takara Bio) for miRNA quantification or with Super Script III reverse transcription poly(dT) first-strand synthesis (Thermo Fisher Scientific) for *Dgcr8* quantification. miRNA primers for the Mir-X qPCR consisted of the full, mature miRNA sequence. Primers for *Dgcr8* were previously reported (Bronevetsky et al., 2013). The qPCR cycle was a two-step cycle at 95°C for 10 s and 60°C for 15 s for 40 cycles, and amplification was read out by SYBR Green Advantage (Takara Bio).

RNA-seq library preparation and sequencing were performed through the University of California, San Francisco, Functional Genomics Core and aligned to the Ensembl mouse GRCh38.78 (mm10) genome using STAR software and analyzed using DESeq2 as previously reported. Transcripts with at least a mean normalized count of 12.3 were used in the analysis, resulting in 12,074 annotated Ensembl transcripts.

Ago2-HITS-CLIP library preparation

Libraries were prepared as previously described (Chi et al., 2009; Gagnon et al., 2019; Loeb et al., 2012). Briefly, 10^8 activated B cells/ml (five mice per library) were UV cross-linked at 1 × 400 mJ and 2 × 200 mJ and pelleted. Ago2 immunoprecipitation with 2D4 (Dako) was performed, and protein–RNA complexes were digested with RNase1, 3′ and 5′ adapters were ligated, and cDNA was created from Super Script III reverse transcription. The library was amplified with Phusion Taq polymerase (New England Biolabs) to the peak exponential by qPCR with SYBR Gold (Thermo Fisher Scientific) before being purified of adapter dimer on a 10% Tris-borate-EDTA gel (Bio-Rad Laboratories) and analyzed by a Bioanalyzer micro DNA kit (Agilent). Libraries were combined and sequenced on an Illumina HiSeq 2500 system. Reads were binned based on individual barcodes and aligned to the genome using Bowtie (John Hopkins University). Annotations were made using an in-house aligning algorithm for each library. Libraries were combined by genotype, and combined libraries were used to run dCLIP (Wang et al., 2014) with default settings. All regions more bound in flox libraries or Δ libraries found by dCLIP were intersected with the miR-221/222-3p seed sequence reference BED file (bedtools), and those regions were further binned based on dCLIP internal score >1 or >10 to increase confidence of true binding regions.

In vivo NP-OVA immunization, HDM challenge, and goat anti-IgD serum immunization

Mice were immunized i.p. with 50 μg of NP-OVA(10–16; LGC Biosearch Technologies) mixed in 1:1 PBS:Alum Imject (Thermo Fisher Scientific) in 200 μl, and blood was collected for serum 14 d later. For the HDM model, mice were primed with 25 μg

HDM (Stallergenes Greer) in 50 µl PBS by oropharyngeal aspiration, and, 7 d later, the mice were challenged similarly for 5 consecutive days before being bled at day 14 for serum analysis. Mice were immunized i.p. with 300 µl goat anti-IgD serum (gift from Jason Cyster, University of California, San Francisco, San Francisco, CA), and spleens and inguinal LNs were analyzed 7 d later by flow cytometry. Flow cytometry plots and analysis are of LN samples.

ELISA

Serum was collected by submandibular bleed and microcentrifugation at >18,000 g for 30 min at 4°C. Half area high-binding 96-well plates (Costar) were used for all assays. For total Ig at steady state, plates were coated with goat anti-Ig (2 µg/ml; SouthernBiotech) overnight in coating buffer bicarbonate/carbonate coating buffer (100 mM, pH 9.6). For NP-specific antibody ELISAs, plates were coated with NP-BSA (5 µg/ml; LGC Biosearch Technologies). Diluted serum was added overnight at 4°C or at room temperature for 2 h and detected with biotinylated goat anti-IgG1, anti-IgG3, anti-IgG2b, anti-IgG2c, anti-IgA, or anti-IgM (2 µg/ml; SouthernBiotech) followed by HRP-avidin (1:5,000; SouthernBiotech) and developed with Super AquaBlue ELISA substrate or 3,3′,5,5′-tetramethylbenzidine substrate (Thermo Fisher Scientific) with the manufacturer's recommended absorbance. For total IgE, the process was the same, except that plates were coated with anti-IgE (2 µg/ml, clone R35-72) and detected with biotinylated anti-IgE (2 µg/ml, clone R35-118).

Flow cytometry

For in vivo experiments, single-cell suspensions were prepared from spleens or LNs by gently passing them through 70-µm nylon mesh filters in complete RPMI medium. For bone marrow, long bones were cut at the base, and a 26-gauge needle was used to expel bone marrow into complete RPMI medium. The single-cell suspension was created by resuspending the bone marrow with an 18-gauge needle, and the suspension was filtered through a 70-µm filter. Before staining with antibodies for surface markers, Fc receptors were blocked with anti-CD16/CD32 (2.4G2) and 2% normal rat serum in FACS buffer (PBS + 2% FBS + 2 µm EDTA + 0.01% NaN$_3$). EDTA can reduce background staining of B cells that do not express IgE but can bind it through CD23 in a calcium-sensitive manner (Richards and Katz, 1990; Hibbert et al., 2005). Conjugated antibodies used for FACS and flow cytometry included peridinin chlorophyll protein–cyanine 5.5 (PerCP-Cy5.5) anti-CD3 (17A2), BV605 anti-CD4 (RM4-5); BV605, PE, and PE-Cy7 anti-CD19 (6D5); allophycocyanin (APC) anti-CD19 (eBio1D3); PerCP-Cy5.5 anti-CD43 (1B11); Alexa Fluor 647 and BV510 anti-B220 (RA3-6B2); Alexa Fluor 488 and APC-Cy7 anti-IgM (RMM-1); eFluor 450 and PE anti-IgD (11-26c); PE and APC anti-IgG1 (A85); PerCP-Cy5.5 anti-IgG1 (RMG1-1); biotin anti-IgE (R35-118); unconjugated biotin and PE anti-IgE (RME-1); APC anti-CD138 (281-2); PE-Cy7 anti-CD45.2 (104); PerCP-Cy5.5 anti-CD45.1 (A20); PacBlue anti-CD21/35 (7E9); PE-Cy7 and PE anti-CD23 (B3B4); PE anti-CD93 (AA4.1); and BV711 anti-CD24 (M1/69). Biotin conjugates were detected using BV711 or BV421 streptavidin (BioLegend). Intracellular IgE staining was

performed as previously described (Yang et al., 2012), where live cells were stained with surface antibody stain + 1:20 purified anti-IgE (RME-1) before fixing with BD Cytofix/Cytoperm and staining intracellularly with PE anti-IgE (RME-1). Dead cells were detected using eFluor 780 fixable viability dye (Thermo Fisher Scientific). Flow cytometric analysis was performed on an LSR II or Symphony cytometer or a FACSAria II cell sorter for sorting (all from BD Biosciences). Counts were made by spiking 5–10^3 AccuCount Blank Particles beads (Spherotech) for total cell count per sample/organ.

Dual luciferase assay

Dual luciferase constructs were generated, and an assay was performed as previously reported (Gagnon et al., 2019; Pua et al., 2016). Cells were stimulated and transfected as outlined, and luciferase activity was measured 24 h after transfection with the Dual Luciferase Reporter Assay System (Promega) and a FLUOstar Optima plate reader (BMG Labtech). At least 1 kb of the 3′ UTR of *Cd164*, *Foxp1*, and *Arid1a*, including the putative miR-221/222-3p seed match sequence(s), were cloned into the psiCHECK-2 luciferase reporter construct (Promega). Primers used were as follows: *Foxp1* forward: 5′-TAAGCAGCTCGA GAGCATGGTGACAGGGCTAAG-3′; Foxp1 reverse: 5′-TGCTTA GGCGGCCGCCTCCCCCGCAAAAGACAAAG-3′; Cd164 forward: 5′-TAAGCAGCTCGAGAGATGCCACACAGGGCAATC-3′; Cd164 reverse: 5′-TGCTTAGGCGGCCGCTGCTTGTGCAGCAAGTATGG-3′; Arid1a forward: 5′-TAAGCAGCTCGAGCCTCAGGACCCCACCCT AT-3′; Arid1a reverse: 5′-TGCTTAGGCGGCCGCCACGTGGAA CATATAGTATAAAG-3′.

Software and statistics

Data visualization and statistical calculations were performed using GraphPad Prism. Statistical tests and P values for each experiment are specified in the figure legends. For a single comparison between two groups, a two-tailed Student's *t* test was used (paired or unpaired where mentioned); for multiple comparisons between a preselected control group and all other groups, a one-way ANOVA with Dunnett's square test was used; and for multiple comparisons where all groups were compared, a one-way ANOVA with a Tukey correction for multiple comparisons test was used. Flow cytometric data were analyzed with FlowJo version 10.2. Gene ontology was run using the Metascape analysis software (Zhou et al., 2019). CDF plots were generated using ggplot2, and an MA plot was generated from DESeq2 results on miRNA captured reads in R version 3.3.4. Figures were made in Adobe Illustrator.

Online supplemental material

Fig. S1 provides a further validation of the methods for primary B cell transfection with small RNAs and retesting of top screen candidate miRNAs affecting CSR. Fig. S2 provides data supporting the choice of threshold for dCLIP analysis and the selection of putative direct target genes for functional analysis.

Data availability

RNA-seq and Ago-HITS-CLIP data are available from the Gene Expression Omnibus database (accession no. GSE153811).

Acknowledgments

References

Agarwal, V., G.W. Bell, J.W. Nam, and D.P. Bartel. 2015. Predicting effective microRNA target sites in mammalian mRNAs. *eLife.* 4:e05005. https://doi.org/10.7554/eLife.05005

Babiarz, J.E., J.G. Ruby, Y. Wang, D.P. Bartel, and R. Blelloch. 2008. Mouse ES cells express endogenous shRNAs, siRNAs, and other Microprocessor-independent, Dicer-dependent small RNAs. *Genes Dev.* 22:2773–2785. https://doi.org/10.1101/gad.1705308

Bartel, D.P. 2004. MicroRNAs: genomics, biogenesis, mechanism, and function. *Cell.* 116:281–297. https://doi.org/10.1016/S0092-8674(04)00045-5

Baumjohann, D., R. Kageyama, J.M. Clingan, M.M. Morar, S. Patel, D. de Kouchkovsky, O. Bannard, J.A. Bluestone, M. Matloubian, K.M. Ansel, et al. 2013. The microRNA cluster miR-17~92 promotes TFH cell differentiation and represses subset-inappropriate gene expression. *Nat. Immunol.* 14:840–848. https://doi.org/10.1038/ni.2642

Belver, L., V.G. de Yébenes, and A.R. Ramiro. 2010. MicroRNAs prevent the generation of autoreactive antibodies. *Immunity.* 33:713–722. https://doi.org/10.1016/j.immuni.2010.11.010

Bronevetsky, Y., A.V. Villarino, C.J. Eisley, R. Barbeau, A.J. Barczak, G.A. Heinz, E. Kremmer, V. Heissmeyer, M.T. McManus, D.J. Erle, et al. 2013. T cell activation induces proteasomal degradation of Argonaute and rapid remodeling of the microRNA repertoire. *J. Exp. Med.* 210:417–432. https://doi.org/10.1084/jem.20111717

Busse, W., J. Corren, B.Q. Lanier, M. McAlary, A. Fowler-Taylor, G.D. Cioppa, A. van As, and N. Gupta. 2001. Omalizumab, anti-IgE recombinant humanized monoclonal antibody, for the treatment of severe allergic asthma. *J. Allergy Clin. Immunol.* 108:184–190. https://doi.org/10.1067/mai.2001.117880

Cameron, L., A.S. Gounni, S. Frenkiel, F. Lavigne, D. Vercelli, and Q. Hamid. 2003. SeSμ and SeSγ switch circles in human nasal mucosa following ex vivo allergen challenge: evidence for direct as well as sequential class switch recombination. *J. Immunol.* 171:3816–3822. https://doi.org/10.4049/jimmunol.171.7.3816

Casola, S., G. Cattoretti, N. Uyttersprot, S.B. Koralov, J. Seagal, Z. Hao, A. Waisman, A. Egert, D. Ghitza, and K. Rajewsky. 2006. Tracking germinal center B cells expressing germ-line immunoglobulin γ1 transcripts by conditional gene targeting. *Proc. Natl. Acad. Sci. USA.* 103:7396–7401. https://doi.org/10.1073/pnas.0602353103

Chi, S.W., J.B. Zang, A. Mele, and R.B. Darnell. 2009. Argonaute HITS-CLIP decodes microRNA-mRNA interaction maps. *Nature.* 460:479–486. https://doi.org/10.1038/nature08170

Coffre, M., and S.B. Koralov. 2017. miRNAs in B cell development and lymphomagenesis. *Trends Mol. Med.* 23:721–736. https://doi.org/10.1016/j.molmed.2017.06.001

Crotty, S. 2019. T follicular helper cell biology: a decade of discovery and diseases. *Immunity.* 50:1132–1148. https://doi.org/10.1016/j.immuni.2019.04.011

de Yébenes, V.G., L. Belver, D.G. Pisano, S. González, A. Villasante, C. Croce, L. He, and A.R. Ramiro. 2008. miR-181b negatively regulates activation-induced cytidine deaminase in B cells. *J. Exp. Med.* 205:2199–2206. https://doi.org/10.1084/jem.20080579

Deenick, E.K., J. Hasbold, and P.D. Hodgkin. 1999. Switching to IgG3, IgG2b, and IgA is division linked and independent, revealing a stochastic framework for describing differentiation. *J. Immunol.* 163:4707–4714.

Dekker, J.D., G.V. Baracho, Z. Zhu, G.C. Ippolito, R.J. Schmitz, R.C. Rickert, and H.O. Tucker. 2019. Loss of the FOXP1 transcription factor leads to deregulation of B lymphocyte development and function at multiple stages. *Immunohorizons.* 3:447–462. https://doi.org/10.4049/immunohorizons.1800079

Dorsett, Y., K.M. McBride, M. Jankovic, A. Gazumyan, T.H. Thai, D.F. Robbiani, M. Di Virgilio, B. Reina San-Martin, G. Heidkamp, T.A. Schwickert, et al. 2008. MicroRNA-155 suppresses activation-induced cytidine deaminase-mediated *Myc-Igh* translocation. *Immunity.* 28:630–638. https://doi.org/10.1016/j.immuni.2008.04.002

Feng, X., G.C. Ippolito, L. Tian, K. Wiehagen, S. Oh, A. Sambandam, J. Willen, R.M. Bunte, S.D. Maika, J.V. Harriss, et al. 2010. Foxp1 is an essential transcriptional regulator for the generation of quiescent naive T cells during thymocyte development. *Blood.* 115:510–518. https://doi.org/10.1182/blood-2009-07-232694

Feng, X., H. Wang, H. Takata, T.J. Day, J. Willen, and H. Hu. 2011. Transcription factor Foxp1 exerts essential cell-intrinsic regulation of the quiescence of naive T cells. *Nat. Immunol.* 12:544–550. https://doi.org/10.1038/ni.2034

Finkelman, F.D., C.M. Snapper, J.D. Mountz, and I.M. Katona. 1987. Polyclonal activation of the murine immune system by a goat antibody to mouse IgD. IX. Induction of a polyclonal IgE response. *J. Immunol.* 138:2826–2830.

Finkelman, F.D., J. Holmes, I.M. Katona, J.F. Urban Jr., M.P. Beckmann, L.S. Park, K.A. Schooley, R.L. Coffman, T.R. Mosmann, and W.E. Paul. 1990. Lymphokine control of in vivo immunoglobulin isotype selection. *Annu. Rev. Immunol.* 8:303–333. https://doi.org/10.1146/annurev.iy.08.040190.001511

Fornari, F., L. Gramantieri, M. Ferracin, A. Veronese, S. Sabbioni, G.A. Calin, G.L. Grazi, C. Giovannini, C.M. Croce, L. Bolondi, et al. 2008. MiR-221 controls CDKN1C/p57 and CDKN1B/p27 expression in human hepatocellular carcinoma. *Oncogene.* 27:5651–5661. https://doi.org/10.1038/onc.2008.178

Fowler, T., A.S. Garruss, A. Ghosh, S. De, K.G. Becker, W.H. Wood, M.T. Weirauch, S.T. Smale, B. Aronow, R. Sen, et al. 2015. Divergence of transcriptional landscape occurs early in B cell activation. *Epigenetics Chromatin.* 8:20. https://doi.org/10.1186/s13072-015-0012-x

Froidure, A., J. Mouthuy, S.R. Durham, P. Chanez, Y. Sibille, and C. Pilette. 2016. Asthma phenotypes and IgE responses. *Eur. Respir. J.* 47:304–319. https://doi.org/10.1183/13993003.01824-2014

Gagnon, J.D., R. Kageyama, H.M. Shehata, M.S. Fassett, D.J. Mar, E.J. Wigton, K. Johansson, A.J. Litterman, P. Odorizzi, D. Simeonov, et al. 2019. miR-15/16 restrain memory T cell differentiation, cell cycle, and survival. *Cell Rep.* 28:2169–2181.e4. https://doi.org/10.1016/j.celrep.2019.07.064

Galardi, S., N. Mercatelli, E. Giorda, S. Massalini, G.V. Frajese, S.A. Ciafrè, and M.G. Farace. 2007. miR-221 and miR-222 expression affects the proliferation potential of human prostate carcinoma cell lines by targeting p27Kip1. *J. Biol. Chem.* 282:23716–23724. https://doi.org/10.1074/jbc.M701805200

Galli, S.J., and M. Tsai. 2012. IgE and mast cells in allergic disease. *Nat. Med.* 18:693–704. https://doi.org/10.1038/nm.2755

Gao, X., P. Tate, P. Hu, R. Tjian, W.C. Skarnes, and Z. Wang. 2008. ES cell pluripotency and germ-layer formation require the SWI/SNF chromatin remodeling component BAF250a. *Proc. Natl. Acad. Sci. USA.* 105:6656–6661. https://doi.org/10.1073/pnas.0801802105

Han, L., V. Madan, A. Mayakonda, P. Dakle, T.W. Woon, P. Shyamsunder, H.B.M. Nordin, Z. Cao, J. Sundaresan, I. Lei, et al. 2019. Chromatin remodeling mediated by ARID1A is indispensable for normal hematopoiesis in mice. *Leukemia.* 33:2291–2305. https://doi.org/10.1038/s41375-019-0438-4

Hibbert, R.G., P. Teriete, G.J. Grundy, R.L. Beavil, R. Reljic, V.M. Holers, J.P. Hannan, B.J. Sutton, H.J. Gould, and J.M. McDonnell. 2005. The structure of human CD23 and its interactions with IgE and CD21. *J. Exp. Med.* 202:751–760. https://doi.org/10.1084/jem.20050811

Hodgkin, P.D., J.H. Lee, and A.B. Lyons. 1996. B cell differentiation and isotype switching is related to division cycle number. *J. Exp. Med.* 184:277–281. https://doi.org/10.1084/jem.184.1.277

Hsin, J.P., Y. Lu, G.B. Loeb, C.S. Leslie, and A.Y. Rudensky. 2018. The effect of cellular context on miR-155-mediated gene regulation in four major immune cell types. *Nat. Immunol.* 19:1137–1145. https://doi.org/10.1038/s41590-018-0208-x

Hu, H., B. Wang, M. Borde, J. Nardone, S. Maika, L. Allred, P.W. Tucker, and A. Rao. 2006. Foxp1 is an essential transcriptional regulator of B cell development. *Nat. Immunol.* 7:819–826. https://doi.org/10.1038/ni1358

Hu, J., J. Chen, L. Ye, Z. Cai, J. Sun, and K. Ji. 2018. Anti-IgE therapy for IgE-mediated allergic diseases: from neutralizing IgE antibodies to eliminating IgE+ B cells. *Clin. Transl. Allergy.* 8:27. https://doi.org/10.1186/s13601-018-0213-z

Jin, H.Y., H. Oda, M. Lai, R.L. Skalsky, K. Bethel, J. Shepherd, S.G. Kang, W.H. Liu, M. Sabouri-Ghomi, B.R. Cullen, et al. 2013. MicroRNA-17∼92 plays a causative role in lymphomagenesis by coordinating multiple oncogenic pathways. *EMBO J.* 32:2377–2391. https://doi.org/10.1038/emboj.2013.178

Jonas, S., and E. Izaurralde. 2015. Towards a molecular understanding of microRNA-mediated gene silencing. *Nat. Rev. Genet.* 16:421–433. https://doi.org/10.1038/nrg3965

Kang, S.G., W.H. Liu, P. Lu, H.Y. Jin, H.W. Lim, J. Shepherd, D. Fremgen, E. Verdin, M.B. Oldstone, H. Qi, et al. 2013. MicroRNAs of the miR-17∼92 family are critical regulators of T(FH) differentiation. *Nat. Immunol.* 14:849–857. https://doi.org/10.1038/ni.2648

Kawabe, T., T. Naka, K. Yoshida, T. Tanaka, H. Fujiwara, S. Suematsu, N. Yoshida, T. Kishimoto, and H. Kikutani. 1994. The immune responses in CD40-deficient mice: impaired immunoglobulin class switching and germinal center formation. *Immunity.* 1:167–178. https://doi.org/10.1016/1074-7613(94)90095-7

Knoll, M., S. Simmons, C. Bouquet, J.R. Grün, and F. Melchers. 2013. miR-221 redirects precursor B cells to the BM and regulates their residence. *Eur. J. Immunol.* 43:2497–2506. https://doi.org/10.1002/eji.201343367

Kopf, M., G. Le Gros, M. Bachmann, M.C. Lamers, H. Bluethmann, and G. Köhler. 1993. Disruption of the murine IL-4 gene blocks Th2 cytokine responses. *Nature.* 362:245–248. https://doi.org/10.1038/362245a0

Koralov, S.B., S.A. Muljo, G.R. Galler, A. Krek, T. Chakraborty, C. Kanellopoulou, K. Jensen, B.S. Cobb, M. Merkenschlager, N. Rajewsky, et al. 2008. Dicer ablation affects antibody diversity and cell survival in the B lymphocyte lineage. *Cell.* 132:860–874. https://doi.org/10.1016/j.cell.2008.02.020

Kraus, M., M.B. Alimzhanov, N. Rajewsky, and K. Rajewsky. 2004. Survival of resting mature B lymphocytes depends on BCR signaling via the Igα/β heterodimer. *Cell.* 117:787–800. https://doi.org/10.1016/j.cell.2004.05.014

Kuchen, S., W. Resch, A. Yamane, N. Kuo, Z. Li, T. Chakraborty, L. Wei, A. Laurence, T. Yasuda, S. Peng, et al. 2010. Regulation of microRNA expression and abundance during lymphopoiesis. *Immunity.* 32:828–839. https://doi.org/10.1016/j.immuni.2010.05.009

Kühn, R., K. Rajewsky, and W. Müller. 1991. Generation and analysis of interleukin-4 deficient mice. *Science.* 254:707–710. https://doi.org/10.1126/science.1948049

Loeb, G.B., A.A. Khan, D. Canner, J.B. Hiatt, J. Shendure, R.B. Darnell, C.S. Leslie, and A.Y. Rudensky. 2012. Transcriptome-wide miR-155 binding map reveals widespread noncanonical microRNA targeting. *Mol. Cell.* 48:760–770. https://doi.org/10.1016/j.molcel.2012.10.002

Lupini, L., C. Bassi, M. Ferracin, N. Bartonicek, L. D'Abundo, B. Zagatti, E. Callegari, G. Musa, F. Moshiri, L. Gramantieri, et al. 2013. miR-221 affects multiple cancer pathways by modulating the level of hundreds messenger RNAs. *Front. Genet.* 4:64. https://doi.org/10.3389/fgene.2013.00064

Mandler, R., F.D. Finkelman, A.D. Levine, and C.M. Snapper. 1993. IL-4 induction of IgE class switching by lipopolysaccharide-activated murine B cells occurs predominantly through sequential switching. *J. Immunol.* 150:407–418.

Marian, C.A., M. Stoszko, L. Wang, M.W. Leighty, E. de Crignis, C.A. Maschinot, J. Gatchalian, B.C. Carter, B. Chowdhury, D.C. Hargreaves, et al. 2018. Small molecule targeting of specific BAF (mSWI/SNF) complexes for HIV latency reversal. *Cell Chem. Biol.* 25:1443–1455.e14. https://doi.org/10.1016/j.chembiol.2018.08.004

Mayeda, A., J. Badolato, R. Kobayashi, M.Q. Zhang, E.M. Gardiner, and A.R. Krainer. 1999. Purification and characterization of human RNPS1: a general activator of pre-mRNA splicing. *EMBO J.* 18:4560–4570. https://doi.org/10.1093/emboj/18.16.4560

Mayoral, R.J., M.E. Pipkin, M. Pachkov, E. van Nimwegen, A. Rao, and S. Monticelli. 2009. MicroRNA-221-222 regulate the cell cycle in mast cells. *J. Immunol.* 182:433–445. https://doi.org/10.4049/jimmunol.182.1.433

Mayoral, R.J., L. Deho, N. Rusca, N. Bartonicek, H.K. Saini, A.J. Enright, and S. Monticelli. 2011. MiR-221 influences effector functions and actin cytoskeleton in mast cells. *PLoS One.* 6:e26133. https://doi.org/10.1371/journal.pone.0026133

Monticelli, S., K.M. Ansel, C. Xiao, N.D. Socci, A.M. Krichevsky, T.H. Thai, N. Rajewsky, D.S. Marks, C. Sander, K. Rajewsky, et al. 2005. MicroRNA profiling of the murine hematopoietic system. *Genome Biol.* 6:R71. https://doi.org/10.1186/gb-2005-6-8-r71

Nojima, T., K. Haniuda, T. Moutai, M. Matsudaira, S. Mizokawa, I. Shiratori, T. Azuma, and D. Kitamura. 2011. In-vitro derived germinal centre B cells differentially generate memory B or plasma cells in vivo. *Nat. Commun.* 2:465. https://doi.org/10.1038/ncomms1475

Nonoyama, S., D. Hollenbaugh, A. Aruffo, J.A. Ledbetter, and H.D. Ochs. 1993. B cell activation via CD40 is required for specific antibody production by antigen-stimulated human B cells. *J. Exp. Med.* 178:1097–1102. https://doi.org/10.1084/jem.178.3.1097

Okada, T., S. Moriyama, and M. Kitano. 2012. Differentiation of germinal center B cells and follicular helper T cells as viewed by tracking Bcl6 expression dynamics. *Immunol. Rev.* 247:120–132. https://doi.org/10.1111/j.1600-065X.2012.01120.x

Patzelt, T., S.J. Keppler, O. Gorka, S. Thoene, T. Wartewig, M. Reth, I. Förster, R. Lang, M. Buchner, and J. Ruland. 2018. Foxp1 controls mature B cell survival and the development of follicular and B-1 B cells. *Proc. Natl. Acad. Sci. USA.* 115:3120–3125. https://doi.org/10.1073/pnas.1711335115

Pérez-García, A., E. Marina-Zárate, A.F. Álvarez-Prado, J.M. Ligos, N. Galjart, and A.R. Ramiro. 2017. CTCF orchestrates the germinal centre transcriptional program and prevents premature plasma cell differentiation. *Nat. Commun.* 8:16067. https://doi.org/10.1038/ncomms16067

Petkau, G., Y. Kawano, I. Wolf, M. Knoll, and F. Melchers. 2018. MiR221 promotes precursor B-cell retention in the bone marrow by amplifying the PI3K-signaling pathway in mice. *Eur. J. Immunol.* 48:975–989. https://doi.org/10.1002/eji.201747354

Pua, H.H., D.F. Steiner, S. Patel, J.R. Gonzalez, J.F. Ortiz-Carpena, R. Kageyama, N.T. Chiou, A. Gallman, D. de Kouchkovsky, L.T. Jeker, et al. 2016. MicroRNAs 24 and 27 suppress allergic inflammation and target a network of regulators of T helper 2 cell-associated cytokine production. *Immunity.* 44:821–832. https://doi.org/10.1016/j.immuni.2016.01.003

Rao, P.K., Y. Toyama, H.R. Chiang, S. Gupta, M. Bauer, R. Medvid, F. Reinhardt, R. Liao, M. Krieger, R. Jaenisch, et al. 2009. Loss of cardiac microRNA-mediated regulation leads to dilated cardiomyopathy and heart failure. *Circ. Res.* 105:585–594. https://doi.org/10.1161/CIRCRESAHA.109.200451

Richards, M.L., and D.H. Katz. 1990. The binding of IgE to murine FcεRII is calcium-dependent but not inhibited by carbohydrate. *J. Immunol.* 144: 2638–2646.

Rodriguez, A., E. Vigorito, S. Clare, M.V. Warren, P. Couttet, D.R. Soond, S. van Dongen, R.J. Grocock, P.P. Das, E.A. Miska, et al. 2007. Requirement of bic/microRNA-155 for normal immune function. *Science.* 316:608–611. https://doi.org/10.1126/science.1139253

Ruzankina, Y., C. Pinzon-Guzman, A. Asare, T. Ong, L. Pontano, G. Cotsarelis, V.P. Zediak, M. Velez, A. Bhandoola, and E.J. Brown. 2007. Deletion of the developmentally essential gene ATR in adult mice leads to age-related phenotypes and stem cell loss. *Cell Stem Cell.* 1:113–126. https://doi.org/10.1016/j.stem.2007.03.002

Sagardoy, A., J.I. Martinez-Ferrandis, S. Roa, K.L. Bunting, M.A. Aznar, O. Elemento, R. Shaknovich, L. Fontán, V. Fresquet, I. Perez-Roger, et al. 2013. Downregulation of FOXP1 is required during germinal center B-cell function. *Blood.* 121:4311–4320. https://doi.org/10.1182/blood-2012-10-462846

Seo, G.Y., Y.S. Jang, H.A. Kim, M.R. Lee, M.H. Park, S.R. Park, J.M. Lee, J. Choe, and P.H. Kim. 2013. Retinoic acid, acting as a highly specific IgA isotype switch factor, cooperates with TGF-β1 to enhance the overall IgA response. *J. Leukoc. Biol.* 94:325–335. https://doi.org/10.1189/jlb.0313128

Shi, Y., S. Gao, Y. Zheng, M. Yao, and F. Ruan. 2019. LncRNA CASC15 functions as an unfavorable predictor of ovarian cancer prognosis and inhibits tumor progression through regulation of miR-221/ARID1A axis. *OncoTargets Ther.* 12:8725–8736. https://doi.org/10.2147/OTT.S219900

Srinivas, S., T. Watanabe, C.S. Lin, C.M. William, Y. Tanabe, T.M. Jessell, and F. Costantini. 2001. Cre reporter strains produced by targeted insertion of EYFP and ECFP into the ROSA26 locus. *BMC Dev. Biol.* 1:4. https://doi.org/10.1186/1471-213X-1-4

Stavnezer, J., and C.E. Schrader. 2014. IgH chain class switch recombination: mechanism and regulation. *J. Immunol.* 193:5370–5378. https://doi.org/10.4049/jimmunol.1401849

Steiner, D.F., M.F. Thomas, J.K. Hu, Z. Yang, J.E. Babiarz, C.D. Allen, M. Matloubian, R. Blelloch, and K.M. Ansel. 2011. MicroRNA-29 regulates T-box transcription factors and interferon-γ production in helper T cells. *Immunity.* 35:169–181. https://doi.org/10.1016/j.immuni.2011.07.009

Teng, G., P. Hakimpour, P. Landgraf, A. Rice, T. Tuschl, R. Casellas, and F.N. Papavasiliou. 2008. MicroRNA-155 is a negative regulator of activation-induced cytidine deaminase. *Immunity.* 28:621–629. https://doi.org/10.1016/j.immuni.2008.03.015

Thai, T.H., D.P. Calado, S. Casola, K.M. Ansel, C. Xiao, Y. Xue, A. Murphy, D. Frendewey, D. Valenzuela, J.L. Kutok, et al. 2007. Regulation of the germinal center response by microRNA-155. *Science.* 316:604–608. https://doi.org/10.1126/science.1141229

Thomas-Claudepierre, A.S., E. Schiavo, V. Heyer, M. Fournier, A. Page, I. Robert, and B. Reina-San-Martin. 2013. The cohesin complex regulates immunoglobulin class switch recombination. *J. Exp. Med.* 210: 2495–2502. https://doi.org/10.1084/jem.20130166

van Keimpema, M., L.J. Grüneberg, M. Mokry, R. van Boxtel, M.C. van Zelm, P. Coffer, S.T. Pals, and M. Spaargaren. 2015. The forkhead transcription factor FOXP1 represses human plasma cell differentiation. *Blood.* 126: 2098–2109. https://doi.org/10.1182/blood-2015-02-626176

Vigorito, E., K.L. Perks, C. Abreu-Goodger, S. Bunting, Z. Xiang, S. Kohlhaas, P.P. Das, E.A. Miska, A. Rodriguez, A. Bradley, et al. 2007. MicroRNA-155 regulates the generation of immunoglobulin class-switched plasma cells. *Immunity.* 27:847–859. https://doi.org/10.1016/j.immuni.2007.10.009

Wang, Y., S. Baskerville, A. Shenoy, J.E. Babiarz, L. Baehner, and R. Blelloch. 2008. Embryonic stem cell-specific microRNAs regulate the G_1-S transition and promote rapid proliferation. *Nat. Genet.* 40:1478–1483. https://doi.org/10.1038/ng.250

Wang, T., Y. Xie, and G. Xiao. 2014. dCLIP: a computational approach for comparative CLIP-seq analyses. *Genome Biol.* 15:R11. https://doi.org/10.1186/gb-2014-15-1-r11

Xu, S., X. Ou, J. Huo, K. Lim, Y. Huang, S. Chee, and K.P. Lam. 2015. Mir-17-92 regulates bone marrow homing of plasma cells and production of immunoglobulin G2c. *Nat. Commun.* 6:6764. https://doi.org/10.1038/ncomms7764

Yang, Z., B.M. Sullivan, and C.D. Allen. 2012. Fluorescent in vivo detection reveals that IgE$^+$ B cells are restrained by an intrinsic cell fate predisposition. *Immunity.* 36:857–872. https://doi.org/10.1016/j.immuni.2012.02.009

Yang, Y., X. Zhao, and H.X. Li. 2016. MiR-221 and miR-222 simultaneously target ARID1A and enhance proliferation and invasion of cervical cancer cells. *Eur. Rev. Med. Pharmacol. Sci.* 20:1509–1515.

Yang, Z., C.M. Wu, S. Targ, and C.D.C. Allen. 2020. IL-21 is a broad negative regulator of IgE class switch recombination in mouse and human B cells. *J. Exp. Med.* 217:e20190472. https://doi.org/10.1084/jem.20190472

Yewdell, W.T., and J. Chaudhuri. 2017. A transcriptional serenAID: the role of noncoding RNAs in class switch recombination. *Int. Immunol.* 29: 183–196. https://doi.org/10.1093/intimm/dxx027

Yoshida, K., M. Matsuoka, S. Usuda, A. Mori, K. Ishizaka, and H. Sakano. 1990. Immunoglobulin switch circular DNA in the mouse infected with *Nippostrongylus brasiliensis*: evidence for successive class switching from μ to ε via γ1. *Proc. Natl. Acad. Sci. USA.* 87:7829–7833. https://doi.org/10.1073/pnas.87.20.7829

Yu, K., and M.R. Lieber. 2019. Current insights into the mechanism of mammalian immunoglobulin class switch recombination. *Crit. Rev. Biochem. Mol. Biol.* 54:333–351. https://doi.org/10.1080/10409238.2019.1659227

Zhang, J., D.D. Jima, C. Jacobs, R. Fischer, E. Gottwein, G. Huang, P.L. Lugar, A.S. Lagoo, D.A. Rizzieri, D.R. Friedman, et al. 2009. Patterns of microRNA expression characterize stages of human B-cell differentiation. *Blood.* 113:4586–4594. https://doi.org/10.1182/blood-2008-09-178186

Zhang, X., Y. Zhang, Z. Ba, N. Kyritsis, R. Casellas, and F.W. Alt. 2019. Fundamental roles of chromatin loop extrusion in antibody class switching. *Nature.* 575:385–389. https://doi.org/10.1038/s41586-019-1723-0

Zhou, Y., B. Zhou, L. Pache, M. Chang, A.H. Khodabakhshi, O. Tanaseichuk, C. Benner, and S.K. Chanda. 2019. Metascape provides a biologist-oriented resource for the analysis of systems-level datasets. *Nat. Commun.* 10: 1523. https://doi.org/10.1038/s41467-019-09234-6
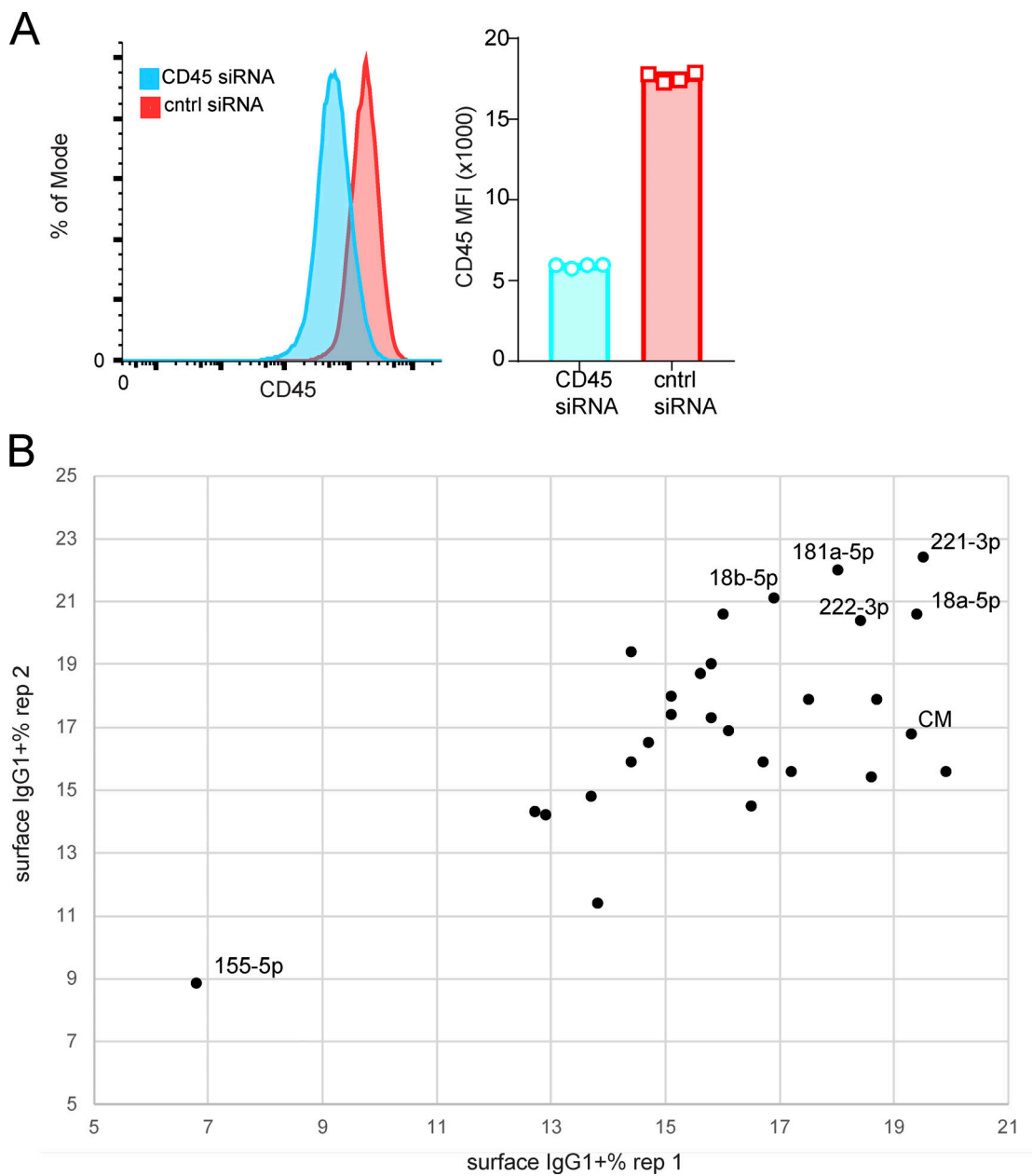
Figure S1. **Extended validation of model, transfection method, and miRNA candidates. (A)** Flow cytometry histograms and quantification of CD45 expression on B cells stimulated in conditions outlined in Fig. 1 A and transfected with CD45 siRNA or control siRNA. Representative of three independent experiments. MFI, mean fluorescence intensity. **(B)** Follow-up rescreen of top 10 and bottom 10 Z-score miRNAs from original screen, transfected in duplicate over two replicates.

A dCLIP differential >1

454 | 80 | 467

flox: 652 peaks
in 534 genes

Δ: 636 peaks
in 547 genes

B dCLIP differential >10

335 | 8 | 49

flox: 412 peaks
in 343 genes

Δ: 61 peaks
in 57 genes

C flox_up_dCLIP intersection
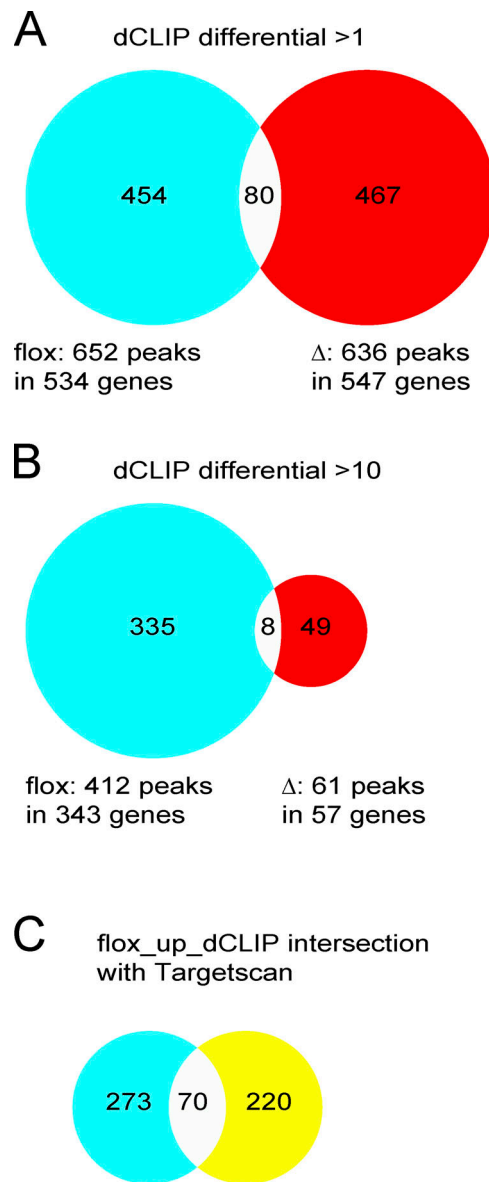with Targetscan

273 | 70 | 220

Figure S2.   **Validation scheme for dCLIP analysis cutoff and selection of targets based on intersection of dCLIP and TargetScan. (A and B)** Total number of genes containing an miR-221/222 seed sequence (6-mer or better) in a region with more binding for flox library (aqua) or Δ library (red) or genes having a region for both genotypes (white) when filtering on a dCLIP internal parameter of 1 (A) or 10 (B). **(C)** Of the 343 genes from B (aqua + white), those that intersect with the 290 genes predicted to be miR-221/222-3p targets by TargetScan (yellow) were selected as siRNA screen candidates (white).